STUDY OF CRYOGENIC STORAGE ON THE MOON

Prepared by

ARTHUR D. LITTLE, INC.
CAMBRIDGE, MASSACHUSETTS

For

NATIONAL AERONAUTICS AND SPACE ADMINISTRATION
GEORGE C. MARSHALL SPACE FLIGHT CENTER
HUNTSVILLE, ALABAMA

Contract NAS8—11377

December 1965

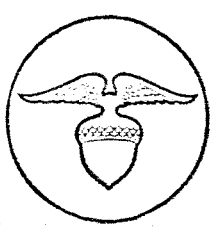

Arthur D. Little, Inc.

STUDY OF CRYOGENIC STORAGE ON THE MOON

Peter E. Glaser
Peter F. Strong
Frank Gabron
Carol H. Sox

ARTHUR D. LITTLE, INC.

CAMBRIDGE, MASSACHUSETTS

December 1965

Contract NAS8-11377

NATIONAL AERONAUTICS AND SPACE ADMINISTRATION

GEORGE C. MARSHALL SPACE FLIGHT CENTER

HUNTSVILLE, ALABAMA

Arthur D. Little, Inc.

TABLE OF CONTENTS

TABLE OF CONTENTS cont'd

LIST OF FIGURES

LIST OF FIGURES (continued)

LIST OF TABLES

I. SUMMARY

This report summarizes the work accomplished during the period from June 27, 1964, to December 31, 1965, on the analysis of the storage problems anticipated in maintaining cryogenic fluids on the surface of the moon in a liquid phase for an extended period of time.

A. PURPOSE

The primary objectives of this program were: (1) to develop a method for predicting the thermal condition of a storage vessel and its cryogenic contents during exposure to the lunar environment for extended periods and (2) to quantitatively predict the expected boil-off losses. Particular emphasis was placed on identifying the radiation interchange with the lunar surface in terms of the observed lunar surface photometric properties and on comparing these results with the radiation from a surface obeying Lambert's cosine law.

B. APPROACH

The approach used in meeting the objectives of the program has been to summarize the available evidence on (1) the lunar environment (including the nature of the lunar atmosphere), (2) the postulated genesis of the lunar surface layer by the micrometeoroid impacts and solar radiation, and (3) the properties--thermal and photometric--of the lunar surface layer which significantly affect the heat exchange of a cryogenic vessel with the lunar surface. The effects of shadows cast on the lunar surface by the storage vessel and the radiation received by the vessel from nearby lunar terrain were established. Design concepts for the cryogenic vessel structural supports and the performance of multilayer insulations were summarized and a design for a model cryogenic vessel was selected to serve as a basis for the heat analysis calculations.

The relationships governing the heat exchange of the vessel with the lunar surface were derived and methods established to permit evaluation of the magnitude of the heat transferred to the tank and the resultant cryogenic liquid boil-off losses.

C. SIGNIFICANCE OF THE PROGRAM

The significance of the results of this program includes the development of analytical procedures for obtaining the boil-off losses from a cryogenic vessel stored on the lunar surface by taking into account the interaction of the vessel with the lunar surface characterized by the available observational evidence. The results indicate that the magnitude of the total radiant heat flux incident upon the outer shroud of the cryogenic storage vessel is so large, compared to the flux due to sunlight reflected from the lunar surface, that the departure of the photometric function from Lambert's law is of slight importance.

II. INTRODUCTION

Following the initial manned lunar landing, there will be a period of intensive lunar surface exploration. To accomplish the objectives of lunar exploration missions, astronauts will have to be able to stay on the moon for extended periods of time. Therefore, systems to provide shelter and mobility for these astronauts are now under consideration. Design studies of shelters and roving vehicles have indicated that long-term storage of cryogenic fluids, particularly liquid hydrogen, will be essential to the success of projected missions. Cryogenic vessels to be transported to the moon will have to be designed so that they can withstand the various forces acting upon them during launch, space flight, and lunar landing; and store the cryogenic fluids with minimum boil-off losses when exposed to the lunar environment.

To analyze the storage problems anticipated in maintaining cryogenic fluids on the surface of the moon in a liquid phase for an extended period of time, the thermal interactions between the storage vessel and the lunar surface have to be determined. To assess as realistically as possible the extent of this interaction, the properties and characteristics of the lunar surface have to be postulated, a design for the cryogenic storage vessel has to be chosen, and the heat inputs to the vessel during a lunation have to be established. Of particular interest is the contribution of the radiation reflected by the lunar surface to the total heat exchange with the cryogenic storage vessel.

In the following sections, the lunar surface characteristics of importance to cryogenic storage are examined; tank supports, the performance of highly effective thermal insulations, and the treatment of piping penetrations to reduce performance degradation are discussed; analyses of the heat exchange and the computation of environment heat fluxes are presented; and the expected boil-off rate for a specific cryogenic tank design is estimated.

III. EFFECTS OF THE LUNAR ENVIRONMENT

The cryogenic storage vessel will be exposed to the lunar environment. Although there are divergent views on the nature of this environment, considerable evidence has been obtained so that the significant aspects--such as an atmosphere of extremely low pressure, effects of micrometeoroid impact and solar radiation, and the resulting thermal and photometric properties of the lunar surface materials--can be postulated.

A. THE LUNAR ATMOSPHERE

Optical and radiotelescope observations have established an upper limit of the density of the lunar atmosphere and, by inference, possible atmospheric constituents. Dollfus (1956) estimated, from measurements of the polarization of sunlight of the lunar atmosphere, that the maximum lunar atmospheric density is less than 10^{-9} of the terrestrial atmospheric density. Costain et al (1955) measured the diffraction of radiowaves by the lunar atmosphere from the occultation of radiostars by the moon. On the basis of this measurement, the lunar atmospheric density was estimated to be about 100 electrons per cubic centimeter. This electron density corresponds to a density of about 10^{-6} molecules per cubic centimeter, or only about 10^{-13} of the terrestrial density. Actual pressures on the lunar surface have not yet been verified experimentally, but on the basis of available evidence, the pressure of the lunar atmosphere at the surface is assumed to be no higher than 10^{-13} terrestrial atmosphere (10^{-10} torr).

Although the lunar atmosphere in general has a very low pressure, local emanations of gases have been observed (Green, 1965), particularly in the region of the craters Alphonsus and Aristarchus, which indicates the possibility of a localized transient lunar atmosphere at a slightly higher than average pressure. Furthermore, spectroscopic observations of lunar craters have indicated radiation from H atoms and C_2 molecules which may be attributed to volcanic activity (Urey, 1961).

In addition to this possible evidence, other transient constituents of the lunar atmosphere may be residual amounts of radiogenic krypton, xenon, argon, radon, and helium which are being generated within the interior of the moon (Opik and Singer, 1960), plus trace amounts of xenon, helium, neon, and argon which may be produced by cosmic ray bombardment of the surface (Opik, 1962). Gases, liquids, and solids--that is, inert gases, alkalis, the halogens, boron, sulfer, and water--may have been released from the interior of the moon by igneous activity (either past or present) (Green, 1965). If indeed, water vapor has been an important constituent of the defluidization of the moon, ice may have been formed in shadowed crater areas and may be slowly vaporizing (Watson

et al, 1961). The lunar atmosphere will also be enriched by gases released during the impact of meteoroids, subsequent vaporization of the impacting material, and the discharge of any occluded gases within the surface material.

The rapid escape of most of the gases of the transient atmosphere on the lunar surface is assured by the low lunar escape velocity (Opik and Singer, 1960). The composition of any transient lunar atmosphere will depend largely on the production rate of the various gases by the different processes mentioned previously. Although the composition of the atmosphere will be complex and changing, the major constituents are probably water, carbon dioxide, and hydrogen.

The absence of any significant lunar atmosphere will shape and control the characteristics of the lunar surface material. Because the moon lacks an atmosphere, its uppermost surface layer is largely determined by the space environment to which it is exposed.

B. GENESIS OF POSTULATED LUNAR SURFACES

1. Micrometeoroid Impacts

The lunar surface is continually bombarded by high-velocity micrometeoroids. This bombardment is expected to cause comminution of exposed materials and consequent erosion of the moon's surface features (Salisbury and Smalley, 1964). Most of the energy in low-velocity meteoroid impact is expended as shock waves which pulverize the target material and eject a portion of the debris to form a crater in the surface. In the higher-velocity impacts, volatilization at the impact site also contributes significantly to the loss of material. The conversion of kinetic energy to thermal energy is great enough so that the material remains in the molecular form and does not condense on expansion.

Bjork's (1961) calculations of the mass of the projectile that produced Meteor Crater Arizona, indicate ejecta-mass-to-projectile-mass ratios of approximately 10^3 at a meteoroid velocity of 11 km/sec and $10^{3.4}$ at a velocity of 72 km/sec. On the basis of this evidence, an ejecta-mass-to-projectile-mass ratio of 10^3 can be assumed for meteoroid impacts on a solid surface at the median velocity of 15-20 km/sec suggested for lunar meteoroids by Whipple (1961). At these velocities, Gault (1963) estimated, on the basis of laboratory experiments, that a very small percentage of the ejecta, amounting to 3-5 times the infall mass, will escape from the moon; and a similar percentage will be vaporized or melted.

If hypervelocity impacts occur on small targets--that is, if the diameter of the impacting particle is greater than about 0.3 times the thickness of the target particles--scabbing or spalling is an important source of fragmentation (Salisbury and Glaser, 1964). It

has also been hypothesized that the large amount of energy put into a porous, fine-grade target material during hypervelocity impact may be sufficient to cause welding or sintering of the powder (Sytinskaya, 1959). Thus, the lunar surface could be covered with partially fused particles. These particles may be rounded droplets of fused materials, irregular shards or grains of shattered materials, and whisker-like crystals of condensed material with a size assumed to be in the 1-10 micron range (Whipple, 1963). Larger, but less frequent, micrometeoroid impacts would disturb the surface more deeply, perhaps turn some of it over, and bury some of the fine materials at various depths, thus creating a rubble layer.

2. Solar Radiation

Important components of radiation from the sun are nonionizing ultraviolet light, solar x-rays, solar wind, and solar flares. The x-rays are soft and of low intensities. The solar wind consists of a continuous but varying stream of electrons, protons, and heavier particles; protons with energies in the range of 4 Kev may have a flux of 10^8 particles/cm^2 sec. Solar flares, which occur with differing frequencies over the 11-year sunspot cycle, have particles with energies up to 30 Mev; the integrated intensity will generally be about 10^4 particles/cm^2 sec (NASA, 1963). The lunar surface may be partially shielded from the solar wind by the lunar magnetic field (Aranowitz and Milford, 1963). However, the lack of data on the magnitude of the magnetic field has led to the assumption that the more energetic particles in the solar wind reach the lunar surface.

In addition to changing the physical and chemical structure of the surface materials, the bombardment by electrons, protons, and heavier particles will lead to the removal of adsorbed monolayers of different gases and create chemically active sites. The resulting clean surfaces may contribute to the consolidation of small particles present on the surface. Radiation sintering of lunar dust has also been advanced as a consolidating mechanism on the lunar surface (Smoluchowski, 1965).

The basic mechanism that can produce adhesion depends on dispersion forces (van der Waals), chemical bonds, mechanical forces, and electrostatic forces.

The tendency for fine particles of most materials to agglomerate and stick to container walls is a common experience (Meissner et al, 1964). In such cases, the force of attraction is generally considered to be a dispersion force of the London-van der Waals type.

In the related field of sliding friction, it is generally accepted that the cohesive strength of a material is developed over the real area of contact; that is, chemical bonds are formed across the contact interface. The average force between chemical bonds is of the order of a hundred times greater than van der Waals forces at equilibrium

internuclear separations. However, chemical forces decrease exponentially with distance and can be effective only for regions that are in intimate contact.

In contrast to chemical bonding, van der Waals forces dominate the adhesion at separations greater than several atomic radii. The relative contribution of chemical bonds to van der Waals adhesion forces will depend on the normal load. For heavy loads, many areas of contact are formed, resulting in the domination of strong chemical bonds. For light loads, as well as for all surfaces not able to form bonds, the adhesion force will be determined by the amount of material within reach of the long-range van der Waals forces, since the real area of contact will be quite small.

If the lunar surface has been subjected to gas contamination from the moon's interior, adsorption of gases on particle surfaces may have taken place. Physically adsorbed gas layers will have been removed rapidly at the low pressures on the lunar surface. Chemisorbed layers, although not completely removed by the action of vacuum alone, would have been removed by the action of solar radiation on exposed particle surfaces. In the absence of any contaminating gas sources, any fresh surfaces generated by mechanical action (e.g., micrometeoroid impacts) would have remained clean. The topography (i.e., microscopic peaks and valleys) of particle surfaces generated by mechanical action will determine the magnitude of adhesion forces. Surface roughness combined with the presence of submicron particles at contact points will reduce adhesion between particles.

Experimental data indicate that the high vacuum can substantially increase the coefficient of friction, by creating microstrains, and, possibly, forming chemical bonds across the contact area (Glaser, 1964). The high friction will tend to make a falling particle stick at its first contact, resist shearing forces that would produce denser packing, and thus contribute to the formation of complex and intricate structures covering all exposed lunar surfaces. If electrostatic forces are present, electrostatic attraction may determine where a particle lands and thus assist in covering the undersides of overhangs or cavities (Salisbury et al, 1964).

3. Electrostatic Effects

The absence of an atmosphere may be responsible for gross electrification greatly exceeding that which normally could be maintained in an atmosphere; in addition, charge mosaics, normally dissipated by mobility of surface charges, may be established and maintained. The existence of such electrostatic charges has been demonstrated experimentally (Salisbury et al, 1964, and Glaser, 1964). The hazards of dust particles have been recognized, and several mechanisms for generating this charge have been suggested. Grannis (1961), Walker (1962), and Coffman (1963) derived theoretical expressions for the random charge fluctuations to be expected as a result of local statistical variations in the flux of solar electrons and protons and secondary

photoelectrons resulting from ultraviolet radiation. The removal of electrons from silicates by ultraviolet radiation could raise the lunar surface potential to several tenths of volts, relative to the surrounding space, by the escape of high-energy photoelectrons; but those electrons which did not have enough energy to escape from the neighborhood of the moon might form a region of increased electron density just above the surface (Singer and Walker, 1962).

The electrostatic behavior of lunar dust may have several important effects. For instance, the presence of electrostatic attraction between particles of opposite charge may assist in deposition of loose particles on exposed surfaces. Also, particles caused by the counteracting forces of gravitational attraction and electrostatic repulsion may be levitated and moved horizontally. Estimates of the height of a cloud of such particles vary: less than 100 microns (Gehrels, 1964), fractions of a centimeter (Grannis, 1961), several centimeters (Singer and Walker, 1962). However, such a cloud of particles would not exhibit the observed photometric properties requiring the presence of horizontal and vertical sharp-edged barriers (Halajian, 1965).

C. PROPERTIES OF THE LUNAR SURFACE LAYER

1. Thermal Properties

The presence of a complex, intricately structured surface layer has been indicated by the photometric measurements and recent radar radiometric measurements which show that the surface material has a dielectric constant of the order of 1.8 to 2.0 (Hagfors et al, 1965).

This layer is responsible for the sharp lunar surface temperature changes during a lunar month which have been measured by infrared and microwave methods. Infrared temperature-measuring techniques, using cryogenically cooled photoconductive detectors (Shorthill and Saari, 1965, and Low, 1965), have indicated temperatures ranging from 80°K to 390°K. This temperature data has been used for theoretical studies of the heat balance of the lunar surface (Krotikov and Shchuko, 1963, and Ingrao et al, 1965). The thermal parameter of the surface layer, $(k\rho c)^{-1/2}$ (where k is the thermal conductivity, ρ the density, c the specific heat), can be determined from the temperature measurement during a lunation.

Typical values of the thermal parameter range from 1200 to 400 cm^2 $sec^{1/2}$ °C/cal representing a low-density, loosely structured material down to a sintered structure of relatively high compressive strength. The thermal parameter for fine evacuated powders, of the order of 3000, is much higher than that of postulated lunar surface materials. It is more likely that the lunar surface is composed of small particles which have been lightly sintered together, so that the contribution of solid conduction across particle contacts leads to an increase in thermal conductivity to correspond to the above range of thermal parameters.

Table III-I summarizes the results of thermal conductivity measurements of postulated lunar surface particulate materials, vesicular foams, and rocks at pressures down to 10^{-10} (Glaser et al, 1965).

The observed changes in surface temperatures (Low, 1965) indicate that the surface materials may have characteristics corresponding to a loose, lightly sintered structure or a vesicular low-density foam.

2. Photometric Properties

The unique manner in which light is reflected by the surface of the moon has prompted many investigators to carry out photometric measurements of the moon. According to the measurements:

- The moon reflects sunlight towards the earth so that the intensity reaches a sharp maximum at or near full moon.
- The variation of brightness of a region is almost exclusively a function of the lunar phase angle and independent of the location on the lunar sphere or of the type of terrain.
- The albedo is low over most areas of the lunar surface.

These measurements indicate that the physical arrangement of the lunar surface material is different than that of terrestrial surfaces, most of which scatter light in accordance with Lambert's law.

a. Albedo

The results of measurements of the lunar albedo have been covered in the reviews of Barabashov (1962), Baldwin (1962), and Fessenkov (1962).

The face of the full moon appears to be of nearly uniform brightness and its average albedo in the visual spectral range (0.4 to 0.7μ) is 0.073. However, there are areas on the moon's surface which have somewhat lower values of albedo and others which have considerably higher values. The extent of these variations is shown below (Barabashov, 1962).

Lunar Feature	Albedo
Sinus Medii	0.054
Mare Serenitatis	0.070
Mare Imbrium	0.074
Mare Nectaris	0.080
Ptolemaeus	0.108
Aristoteles	0.110
Copernicus	0.120
Tycho	0.137
Tycho, rays	0.163

TABLE III-I

THERMAL PROPERTIES OF FOAMED AND POWDERED MATERIALS

Material	Per cent void space	Density[a] (gm/cm^3)	Specific heat (cal/gm °C)	Thermal conductivity[b] (cal/cm sec °C) X 10^6	Thermal parameter $(k\rho C)^{-1/2}$ (cm^2 $sec^{1/2}$ °C/cal)
Pumicite	49	1.27	0.22	140	160
Basalt lava	25	2.08	0.20	530	68
Sintered perlite (open cells)	88	0.31	0.21	59	510
Perlite, loose 200 μ particles	97	0.08	0.21	5.5	3300
Olivine <70 μ particles	35	2.0	0.19	3.2	910
Granodiorite <20 μ particles	63	1.0	0.19	7.2	850

[a] Density measured in air.

[b] Thermal conductivity measured in vacuum

The maria and ancient "lands" have, in general, low values of albedo while the rims of the most recent craters and the "rays" have the highest values.

In the visible range the moon appears to be very nearly a grey body except for some slight variations in hue from faintly reddish to greenish. On the whole, the albedo tends to increase slightly from the blue to the red and it probably continues to rise in the infrared. This can be inferred from the measurements of Pettit and Nicholson (1930) on the radiant emittance of the moon. For these measurements, the investigators separated the sun's reflected radiation from the total radiation of the moon by means of a water filter in front of their thermocouple. The filter passed radiation in the visible range and cut off effectively all infrared radiation beyond 1.4μ. The fraction of radiation reflected in the visible range, including near infrared, to 1.4μ appeared to be about 0.155 for the central region of the lunar disc. Therefore, the infrared albedo of the moon must be greater than this average value.

The polarization measurements carried out by Dollfus (1952) have narrowed down the number of theoretical models which had been proposed to explain the lunar reflection behavior. These measurements indicate that the lunar surface polarizes the sunlight, that the reflection is characteristic of objects of the order of the sizes of wavelengths of light, and that materials such as volcanic ash can reproduce the lunar polarization measurements.

b. Photometric Function

The values of albedo as reported without other qualifications refer to the full moon observed from the earth. In this special case, the angle of incidence and the angle of observation (equal to the angle of reflection) are always equal. In the more general case of an object receiving radiation in the close vicinity of the lunar surface, the albedo is found to depend on the angle of incidence (i), the angle of reflection (ϕ), and azimuth angle (θ). The dependence of the radiation $I = I(i, \phi, \theta)$ is the photometric function. The lunar albedo follows a photometric function which departs drastically from the commonly known functions, in particular from Lambert's cosine law.

A photometric function which appears to conform very closely with the observed photometric properties of the lunar surface has been derived by Hapke (1963). Hapke's function is given by the following expression:

$$I(i, \phi, \theta) = I_o \, ds \, d\omega \, \frac{2}{3\pi} \, \rho \, \frac{1}{1 + \cos \phi / \cos i} \, \frac{\sin \theta + (\pi - \theta) \cos \theta}{\pi} \cdot B(\theta, g).$$

Here, I denotes the amount of diffusely reflected radiation received by an element of surface, ds, viewing a solid angle, dω, of the lunar surface illuminated by the incident radiation of intensity, I_o.

ϕ is the angle of reflection referred to the normal.

θ is the angle between the directions of incidence and reflection.

ρ is the diffuse reflectivity of the particles constituting the lunar surface.

g is a dimensionless "compaction parameter" related to the packing density of the particles ($g \approx 0.6$ to 0.8).

$B(\theta,g)$ is the "backscattering function",

$$B(\theta,g) = 2 \frac{\tan \theta}{2g}\left(1 - e^{-\frac{g}{\tan \theta}}\right) \cdot \left(3 - e^{-\frac{g}{\tan \theta}}\right),$$

for $\theta \leq \frac{\pi}{2}$

and $B(\theta,g) = 1$ for $\theta \geq \frac{\pi}{2}$.

The backscatter function results physically from shadowing of radiation entering into a loosely packed particulate surface when viewed at angles deviating from the directions other than that of the incident beam. There are numerous assumptions made in the derivation of Hapke's function, which have been justified by the agreement of the computed photometric functions with the experimental data.

To reconcile the different hypotheses which have been advanced to explain the remarkable lunar backscattering, Hapke and Van Horn (1963) carried out measurements which disclosed that materials which scattered light like the moon had a complex porous structure with a random arrangement of objects, large compared with wavelengths of visible light and low reflectivity, and arranged in an open network into which light from any direction can penetrate freely. These objects are located so that the structure on a microscopic scale appears to be an isotropic and homogeneous material. This structure would also be in accord with the postulated genesis of the lunar surface and the thermal properties of such a material. By reproducing the lunar backscattering behavior using hard, highly porous "macro rough" volcanic cinders, scoriae, and slags, Halajian (1965) has shown that the photometric function of a surface depends primarily on the geometry of its elements, not on the actual size of those elements.

In an attempt to simulate the affects of the solar wind on the photometric properties, Hapke (1965) used two kilovolt hydrogen ions to bombard

a wide variety of material. He found that proton irradiation of fine rock particles changed their photometric properties so that they more closely resembled lunar characteristics. Furthermore, in determinations of the photometric properties, the composition of irradiated rock powders did not seem to be critical. Because the albedos of all irradiated rock powders appeared to be about 5%, which is less than the albedo of even the darkest portion of the lunar surface, other processes may be operating on the moon to counteract the darkening process. Chief among these are the stirring by micrometeoroid bombardment to expose new material. Variations in the albedo may not only be due to the material composition but also to the geometry of the material. The structure of the lunar surface may be responsible for changes in absorptivity at different angles of solar incidence (Polgar and Howell, 1965).

c. Emittance

The emittance of the lunar surface has been the subject of considerable conjecture. Recent measurements by Markov and Khokhlova (1965) indicated a variation of emittance ranging from 0.62 for the continents to 0.83 for the maria areas at wavelengths of 3.6 and 8-14 microns. The uncertainties in the assumption of a grey body, even though the observations indicated approximately equal brightness temperatures in the two wavelength regions used, introduced considerable uncertainty in the results. The measurements of the emittance of terrestrial rocks (Lyon and Burns, 1964, and Van Tassel and Simon, 1964) indicated variations from 0.65 to 0.93. Because of the lack of reliable data on the lunar surface emittance and its directional properties, several investigators have assumed that the lunar surface emittance approaches that of a black body (Jaeger, 1953, Krotikov and Shchuko, 1963).

D. EFFECTS OF THE LUNAR ENVIRONMENT ON A CRYOGENIC STORAGE VESSEL

1. Changes in Alpha/Epsilon Ratio Caused by Deposition of Particles

The surface of a cryogenic-liquid storage vessel on the lunar surface could be covered by a layer of particles ejected from the lunar surface by micrometeoroid impacts. The estimates of the rate of accretion of such a layer on any object on the lunar surface are quite uncertain (McCracken and Dubin, 1964). The depth of the particle layer accumulated over a one-year period will be assumed to be in a range between 1μ and 10^{-4}μ. The effect of such a thin, uniform layer of fine particles deposited on the surface of a diffusely reflecting material upon its reflectivity is examined below.

Reflectivity of a plane surface covered with a homogeneous layer of a scattering material characterized by a scattering coefficient s may be calculated, according to Kubelka (1948 and 1954) by the following formula:

$$R = \frac{1-R_o\ (a-b\ \coth\ bsx)}{a+b\ \coth\ bsx\ -\ R_o}\ ;$$

where R_o is the diffuse reflectivity of the material before it has been covered, x is the depth of the scattering layer, $a = 1/2\ (R_s^{-1} + R_s)$, and $b = 1/2\ (R_s^{-1} - R_s)$. R_s is the diffuse reflectivity of the scattering material measured in an infinitely deep layer.

The quantity which is as yet undetermined is the scattering coefficient, s, of the particle layer because the physical parameters of the layer (e.g., particle size, the optical constants, and the volume packing fraction) are unknown. However, to evaluate experimental data of Henry (1948) using the Kubelka theory,we may estimate the magnitude of the coefficients. Henry has measured the spectral transmittance of powder layers consisting of particles of known size and optical constants (quartz and zinc sulfide) deposited in known thickness on a transparent (rocksalt) substrate. By using Kubelka's formula for transmittance of a scattering layer,

$$T = \frac{b}{a\sinh bsx + b\cosh bsx},$$

we may calculate the values of s (or sx) from the measured values of T. The scattering is usually large (i.e., the argument $bsx \gg 1$), in which case, the formula simplifies to

$$T = 2b(a+b)^{-1} \exp(-bsx)$$

and

$$sx + b^{-1} \ln [2b(a+b)^{-1}\ T^{-1}].$$

The value of a (and b) is obtained from the diffuse reflectivity, R_s, of lunar dust material in an infinitely deep layer. If we take for this quantity a lunar albedo figure of, say, 0.15, we obtain

$$a = 3.41,\ b = 3.26.$$

Henry's measurements show that in the spectral range from the visible red to about 3 microns, in which the quartz particles act only as scatterers (their absorption coefficient being nearly zero), the scattering is so great that even for partial coverage (e.g., a 2.3 micron layer "depth" of 6.6 micron particle size) the transmission seldom exceeds a value of 10 per cent. In general, transmission is very low at short wavelengths and it becomes significant only in the vicinity of the restrahlen bands of quartz by the action of the Christiansen filter effect.

We have compiled below some of the transmittance data of quartz dust layers from figures 2 to 4 of Henry (1948).

Transmittance of a Layer of Quartz Particles Deposited on Rocksalt Plates

Particle Size	Layer Depth	T(at 0.8μ)	T(at 2μ)
1.0μ	1.1μ	0.03	0.20
	6.0	0	0.01
	9.6	0	0
	12.6	0	0
6.6μ	2.3μ	0.12	0.07
	3.4	0.03	0.02
	6.2	0.01	0
	14.8	0	0
15.5μ	4.1μ	0.08	0.05
	6.7	0.03	0.02
	14.9	0.01	0.01

The values of sx corresponding to the values of Transmittance T, calculated by the simplified formula given above are listed below.

T	sx
0.01	1.40
0.02	1.19
0.03	1.07
0.05	0.91
0.08	0.77
0.12	0.65

As a numerical example consider a cryogenic storage vessel provided with a thermal control coating having an initial value of diffuse reflectivity $R_o = 0.75$ which collects (after some as yet uncertain time) a layer of quartz-like particles of 1 micron average size, 1.1 micron deep. Then, from the above compilations sx will have a value 1.07 at 0.8 micron wavelength. The reflectivity of the particle-covered surface will then be $R = 0.15$. If we assume that the emissivity of the vessel surface does not change and that $\alpha \approx 1-R$, the alpha/epsilon ratio of the vessel surface will increase by more than a factor of 3, leading to a considerable increase in surface temperature.

These considerations indicate that the effects of particle deposits may adversely influence the performance of the cryogenic storage vessel. However, Kubelka's formulas are derived from a continuum theory and may not be strictly applicable to discontinuous layers such as represented by loose dust particles only partly covering the surface. Moreover, the effect of the particle deposits on the emissivity of the vessel surface would also have to be known.

2. Changes in Surface Properties by Micrometeoroid Impacts

In addition to the possibility of the surface deposition of particles, erosion by micrometeoroids would alter the surface optical properties. The damage by micrometeoroids to the vessel surface may be caused by perforation, partial penetration resulting in the formation of a deep crater or removal of surface material and formation of shallow craters. In considering only micrometeoroid impacts cratering phenomena leading to erosion will be the most likely occurrence with perforations of the material having a much lower probability.

Studies of micrometeoroid erosion on aluminum have indicated that the percentage of the cratered area to the total surface area is about 35% during a six-month exposure of an aluminum surface (Merrill 1965). Bombardment by tungsten microparticles with a velocity of about 1.5 km/sec. indicated that a 100% change in aluminum emittance occurred over the cratered surfaces. In another study (Mirtich and Mark 1965) silicon carbide micron sized particles were used to bombard polished aluminum and aluminum coated Mylar. The reflectance was reduced to about 50% after bombardment in the visible range and to about 75% of the original value between 10 and 15 microns. The reflectance of the aluminum coated Mylar was reduced uniformly to about 55% up to wavelengths of 15 microns. For micrometeoroids of about 10^{-9} grams the reflectance of a polished aluminum surface has been estimated to drop to half of the original value in about three years, while for particles of 10^{-11} grams the damage time would be reduced to about seven months (Mirtich and Mark 1965). Because of the lack of specific data of the effect of micrometeoroid erosion on surface vessel coating, a range of α/ϵ ratios has to be considered in determining the boil-off rate of the cryogenic fluids.

3. Low Pressure Environment

The ambient low pressure to which the cryogenic storage vessel will be exposed on the lunar surface will be most helpful in maintaining the cryogenic fluid within the vessel for extended periods. Through careful design of the thermal insulation the contributions of gas conduction to heat transfer to the cryogenic fluid can be most effectively reduced. Any residual gases or products of outgassing can be vented to the lunar atmosphere assuring the efficient operation of the insulation.

4. Interaction Between the Storage Vessel and the Lunar Surface

The radiation interchange between the surface of the cryogenic storage vessel and the lunar surface for the postulated photometric properties is treated in detail in Section V. By assuming that the lunar surface emittance approaches that of a black body a conservative design approach for the cryogenic storage vessel can be followed. As more specific data on the emittance of the lunar surface is obtained the analyses described in Section V can be modified to take into account specific emittance properties.

IV. CRYOGENIC STORAGE VESSEL DESIGN CONCEPTS

The general function of any cryogenic-liquid storage system is to contain and conserve the stored liquid until such time as it is withdrawn and used. The cryogenic storage vessels to supply lunar roving vehicles and shelters must serve this general function. Containment of liquid hydrogen presents no serious problem. However, the conservation of the cryogenic fluid for extended periods in a simulated lunar environment with minimum boil-off loss has yet to be demonstrated. The low temperature of the stored fluid relative to the environmental temperatures causes a heat flow to the fluid and a subsequent loss. Thus, to conserve the fluid the net heat inflow from the outer boundary to the stored cryogenic fluid must be limited.

In any real system, there are many paths through which heat may be transferred to the stored fluid. The principal one, of course, is the surface of the vessel; this surface must be isolated from the environment by a thermal insulation. Others include the structural supports and piping which interrupt the insulation at several points and conduct heat to localized areas of the vessel surface. The pipes will also radiate heat from their warm ends through their interiors to the stored fluid unless the openings are appropriately baffled. The heat leaks resulting from each source and the heat-source interactions can be estimated using analytical techniques and experimental data now available.

The thermal insulation and design concepts appropriate for a cryogenic storage vessel for use on the lunar surface are discussed in the following sections. A specific design for such a vessel forms the basis for the analysis of the heat exchange of this vessel with the lunar environment.

A. THERMAL PROTECTION SYSTEMS

1. Multilayer Insulations

In recent years, a large variety of multilayer insulations and appropriate analytical techniques to predict their performances have been developed (Timmerhaus, 1958-1965). Table IV-I lists physical properties of typical multilayer insulations which hold promise for application to cryogenic storage vessels.

The heat flux into the cryogenic vessel is influenced by the effects of variables such as:

- warm-boundary temperature,
- compression applied to the insulation during installation and during operation,
- type of gas and gas pressure inside the insulation,
- insulation thickness,

TABLE IV-I

THERMAL CONDUCTIVITY MULTILAYER INSULATION

Multilayer Insulation		Thermal Conductivity 0.001 psi Compression	Density Weight	Thermal Conductivity 15 psi Compression
Thickness (in)	Material	(Btu-in/hr-ft^2-°F)	(lb/ft^2)	(Btu-in/hr-ft^2-°F)
0.002 0.007	1145-H19 Aluminum Nylon Mesh	0.43×10^{-4}	15	160×10^{-4}
0.00025 0.007	Double Coated Aluminized Polyester Film Nylon Mesh	0.58×10^{-4}	3	180×10^{-4}
0.0005 0.001	Soft Aluminum Fiberglas Cloth (3 layers)	0.83×10^{-4}	10	330×10^{-4}
0.0005 0.014	Soft Aluminum Fiberglas Mat	1.0×10^{-4}	5	44×10^{-4}
0.002 0.020	1145-0 Aluminum 1/8 x 1/8 Vinyl Mesh	1.4×10^{-4}	16	-
0.002 0.020	1145-H19 Aluminum 1/8 x 1/8 Vinyl Mesh	1.4×10^{-4}	16	-
0.0001 0.003	Soft Aluminum Fiberglas Mat	1.4×10^{-4}	3	76×10^{-4}
0.00025	Crinkled one-side Aluminized Polyester Film	1.9×10^{-4}	1.4	410×10^{-4}

NOTE: Measurements taken between +70 and -423°F

- radiation shield emittance,
- outgassing,
- venting requirements, and
- material stability.

Figures IV-1, 2, and 3 show the heat flux for a typical multilayer insulation as a function of warm-boundary temperature, gas pressure, and applied compression for a cold boundary temperature of about 21°K.

The thermal conductivity of multilayer insulations for a given set of operating conditions has been shown to be (Little, 1963):

- proportional to the fourth power of the warm-boundary temperature;
- nearly independent of the cold-boundary temperature if the cold-boundary temperature is low compared to the warm-boundary temperature;
- directly proportional to the gas pressure if it is below 1×10^{-4} torr--for pressures above 1×10^{-4} torr quality of a multilayer insulation deteriorates rapidly--and,
- approximately proportional to the 2/3 power of the compressive load applied to the insulation.

To meet specific requirements, a wide variety of multilayer application techniques have been developed. Among the various methods for installations of multilayer insulations are:

- prefabricated blankets made of several radiation shields and spacers preshaped to the contour of the container and placed directly on the tank.
- multilayer insulations shaped and assembled layer-by-layer directly on the tank surface.
- narrow (1 to 3 inches wide) continuous strips of radiation shield and spacer material wrapped on the tank and covering the surface of the tank with a desired number of layers; and
- shingle-type radiation shields and spacers.

2. Types of Thermal Protection Systems

In terrestrial applications, multilayer insulations can be enclosed inside a vacuum-tight outer pressure vessel. In a cryogenic vessel

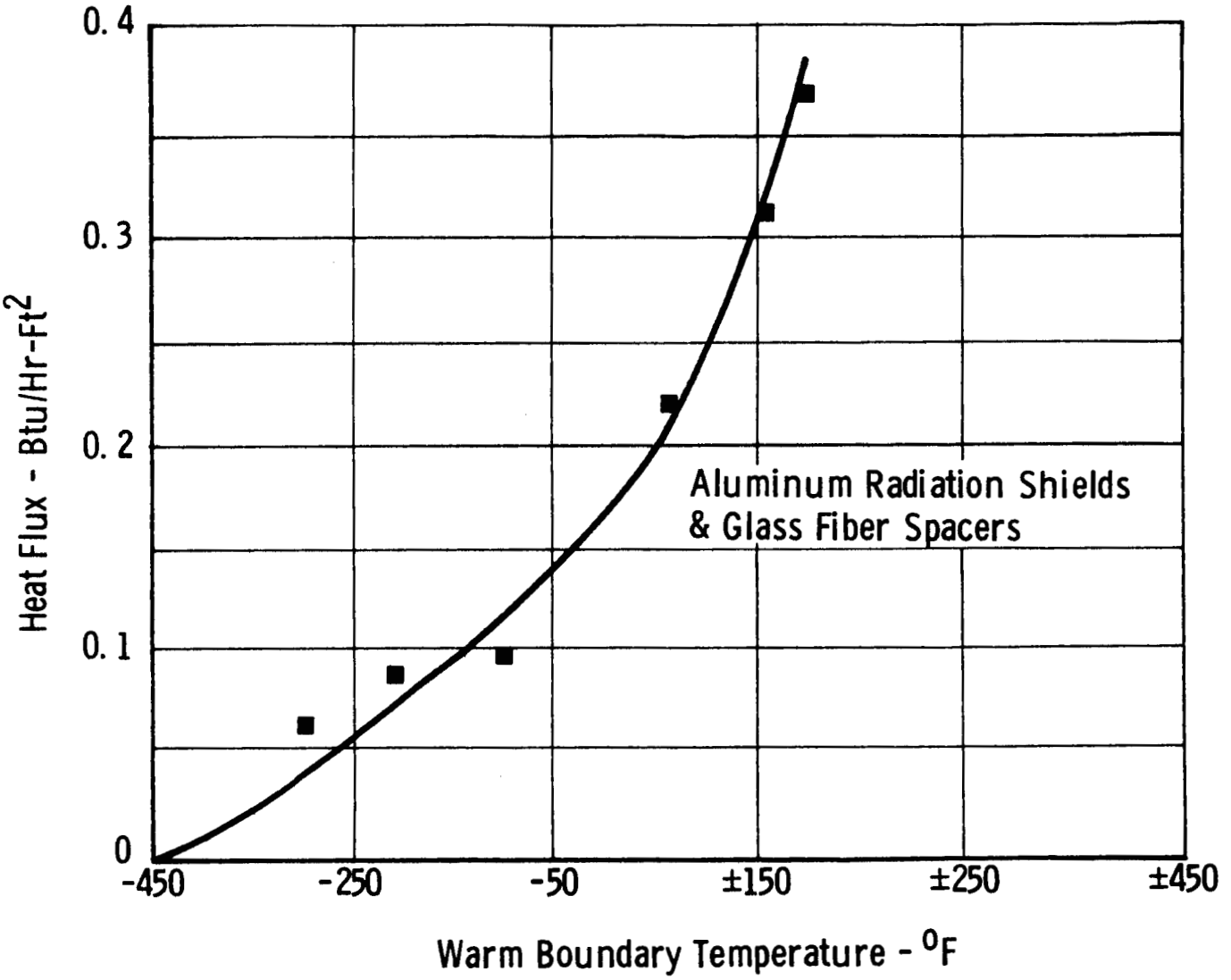

FIGURE IV-1 EFFECTS OF TEMPERATURE ON HEAT FLUX

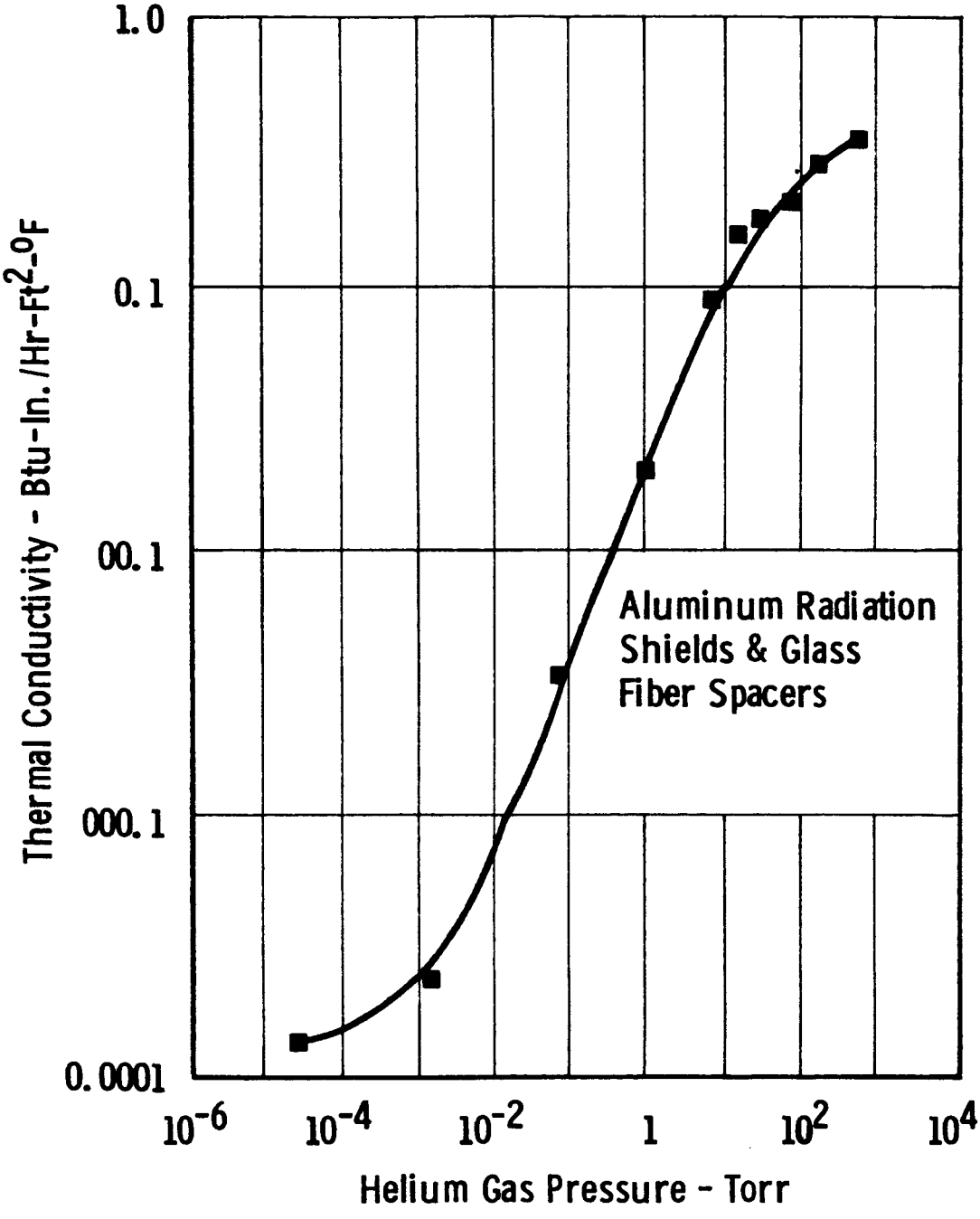

FIGURE IV-2 EFFECTS OF HELIUM GAS PRESSURE ON THERMAL CONDUCTIVITY

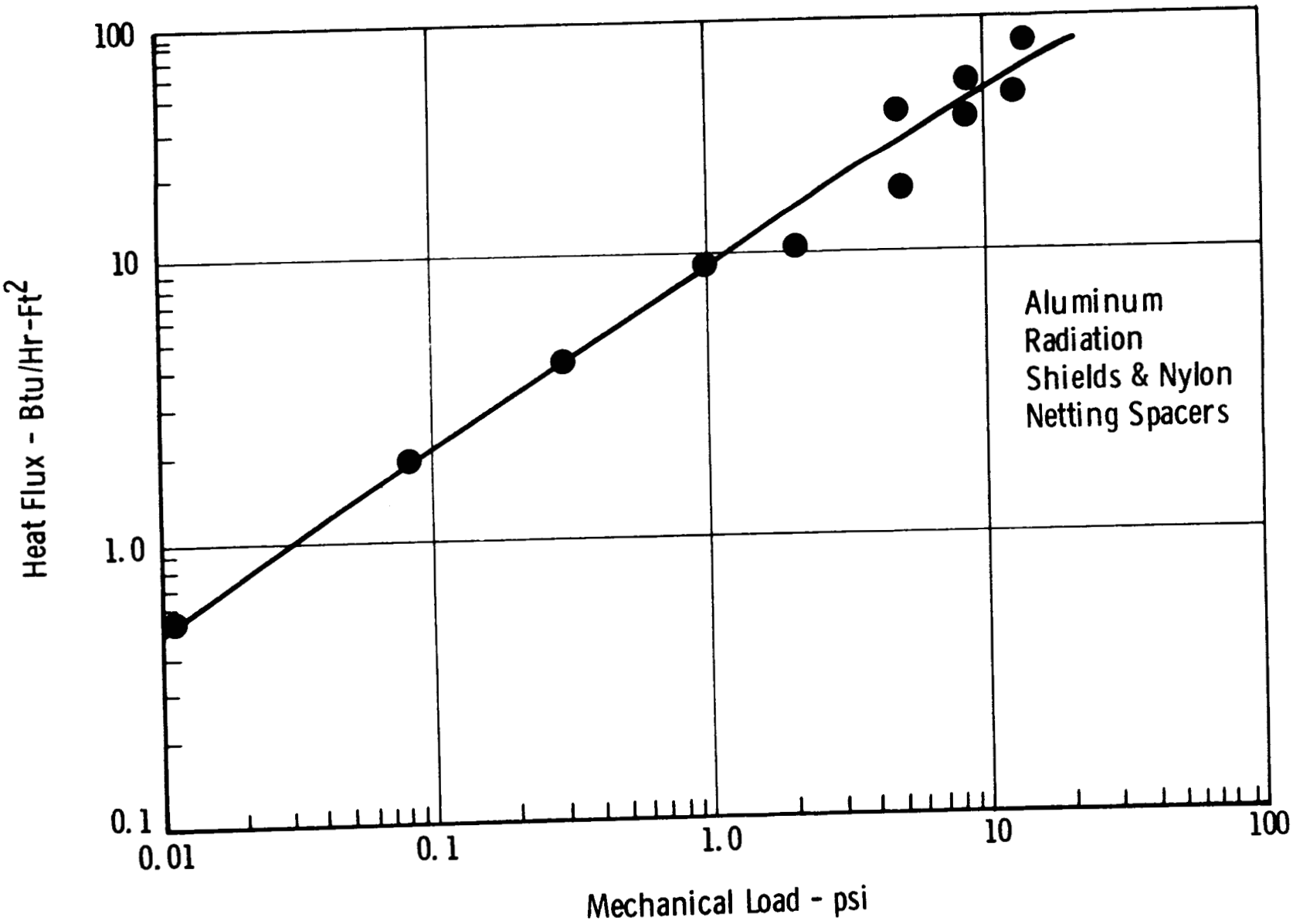

FIGURE IV-3 EFFECTS OF COMPRESSION ON HEAT FLUX

transportable by a space vehicle, the penalty of a heavy outer pressure shell would be prohibitive; therefore, a multilayer insulation must be designed so that it can operate in the different environments acting upon it prior to launch, during boost, in space, during a lunar landing, and during storage on the lunar surface. Considerable work has already been carried out to devise systems which can perform adequately in these different environments. Among these systems are pre-evacuated multilayer insulations using lightweight flexible jacket insulations (Perkins et al., 1964), buckling metal jackets (Leonhard, 1965), a metal jacket with two different series of corrugations perpendicular to each other and regularly spaced in both directions (Gazocean, 1964), and space evacuated systems relying on pumping through seams and edges to the ambient low pressure environment.

As gases boil off from the cryogenic liquid, they have a significant refrigeration potential with respect to the temperatures of the environment and the insulation system. This refrigeration can be used by allowing the boil-off gases to cool the vessel supports, liquid or gas lines, or one or more radiation shields placed in the insulation between the cold wall of the liquid container and the outer warm shroud. A cooled shield can be used to intercept a portion of the heat passing through the insulation and transfer this heat to the vent gas, which will then rise in temperature. The amount of heat thus removed will be proportional to the amount of gas being vented, the specific heat of the gas, and the temperature rise of the gas.

The location of the cooled shield and the magnitude of the reduction of the boil-off have been investigated in a powder insulated liquid hydrogen vessel (Scott, 1959). The improvement in insulating effectiveness obtained with a cooled shield has been extended by analysing the performance of multiple vapor-cooled shields. Paivanos, et al (1965) have analyzed the improvement theoretically obtainable through the use of an infinite number of vapor-cooled shields where every radiation shield is made to serve also as a vapor-cooled shield. With vapor cooling, the boil-off rate of hydrogen can be reduced to 0.19 of the value that would be obtained without vapor cooling.

An analysis of the position of a single cooled shield in a multilayer insulation indicated that the optimum shield location would be within 20 per cent of the insulation thickness from the cold surface (Moore, 1965). The thermal effectiveness is not sensitive to the location of the shield within from 5 to 60 per cent of the insulation thickness. For the optimum shield locations, the boil-off rate of hydrogen can be reduced as much as 0.26 of the value without a shield.

B. STRUCTURAL SUPPORTS

The requirements for supports of the cryogenic vessel will be different for each phase of a specific mission. From earth launch to lunar landing, at intermittent intervals the vessel will experience three-axis accelerations and vibration. The container supports for these conditions will have to be of greater strength and therefore more massive than the supports required during storage on the lunar surface, where the container will experience a gravity force 1/6 that of earth gravity. To minimize heat leaks, it may be desirable to alter the supports to suit the various load conditions, and various material choices and design approaches can be considered to achieve this objective.

1. Materials

Thermal conductivity, tensile strength, and modulus of elasticity are the most significant properties in the design of a support system. A number of candidate structural materials are presented in Table IV-II along with values for each property.

The heat leak per unit of load for a support member in pure tension is proportional to k/σ, where k is the thermal conductivity and σ is the maximum working stress of the member. Using room temperature values of the conductivity and the stress values indicated, we computed k/σ values. Table IV-II shows these values for candidate materials. Among these materials, the industrial yarns, dacron, Nomex and glass fibers have significantly lower values of k/σ than do stainless steel and titanium alloys.

The natural frequency of a support system and cryogenic vessel must be greater than the frequency of any excitations that result from the vibrations and accelerations induced at the time a space vehicle is thrusting. A material will provide minimum conductance support at the natural frequency of a tension support when the ratio of the thermal conductivity of the support to its modulus of elasticity is at a minimum. Also summarized in Table IV-II is the value of this ratio for various materials.

2. Design Concept

Although a number of designs for supports of storage vessels have been used, e.g., tension supports, multiple thermal resistance supports and refrigerated supports, a cone support system has been analyzed and tested in detail (Lockheed, 1965). Experimental results indicate that very good performance on a weight-heat leak basis can be obtained. The cone support can be made of a mylar honeycomb material which is formed to a cone shape and bonded to a girth ring around the inner container and a girth ring on the outer shroud. The cone can be designed to withstand longitudinal accelerations in two directions as well as transverse accelerations for both the tensile and buckling loads associated with such accelerations.

TABLE IV-II

THERMAL AND MECHANICAL PROPERTIES OF SUPPORT MATERIALS

	Modulus of Elasticity $E \times 10^6$ (psi)	Thermal Conductivity k (Btu/hr ft ^{o}F)	Tensile Strength (1000 psi)	k/σ	k/E
Stainless Steel	29.0	8.2	90-285	$0.91\text{-}0.29 \times 10^{-4}$	0.28×10^{-6}
Titanium Alloy (7% Al, 4% Mo)	17.0	4.1	60-170	0.68-0.24	0.24
Pyroceram (9608)	12.5	1.14			0.91
Borosilicate Glass (7740)	9.1	0.65			0.071
Wood - Balsa	0.5	0.03			0.060
Maple	1.8	1.11			0.061
White Pine	1.2	0.087			0.072
Industrial Yarn - Dacron (68)	2.0	0.092	80-145	$1.2\text{ -}0.63 \times 10^{-6}$	0.046
Nylon (702)	0.95	0.14			0.15
Nomex	2.8	0.075	70- 90	$1.1\text{ -}0.84 \times 10^{-6}$	0.027
Epoxies - Cast Unfilled	0.35	0.11			0.31
Glass Filled	3.0	0.2			0.067
Glass Fibers (YM31A)	16.8	0.60	200-220	$3.0\text{-}2.7 \times 10^{-6}$	0.036

Because this type of support penetrates the multilayer insulation, the attachment of the individual layers to the cone has to be accomplished so that the temperatures of the shields match the temperature distribution in the support cone. In this manner, isothermal surfaces can be preserved around the container in the vicinity of the support cone, and thermal short circuits can be prevented. Figure IV-4 shows a design concept for such a support system.

C. DESIGN OF MODEL CRYOGENIC VESSEL

We investigated several design concepts for a model cryogenic vessel as the basis for the calculations of heat interchange on the lunar surface. The following design was chosen because it represents a design based on practical experience, which can be used to demonstrate calculational techniques. Although not optimized, the design is representative of a lunar liquid-hydrogen vessel and illustrates the particular problems associated with storing liquid hydrogen on the lunar surface.

A schematic diagram of the vessel is shown in Figure IV-5. The liquid hydrogen is contained in a 14-foot diameter spherical vessel supported within a cylindrical shroud which rests on a tripod support system. The over-all size and shape of this package were chosen to correspond to the Lunar Excursion Module. The spherical vessel is attached to the main vehicle structure by a single continuous cone and is thermally protected with a multilayer insulation system. All of the piping required to fill, vent, and drain the vessel is arranged to form a single piping penetration on the top of the vessel. A five-foot diameter spherical pressure vessel inside the liquid hydrogen vessel stores high-pressure gaseous helium required to pressurize the ullage space of the vessel during withdrawal of liquid hydrogen.

1. Operation

The general mode of operation requires that the vessel be filled and topped off continuously prior to launch at a pressure somewhat above one atmosphere. This pressure is maintained by a low pressure vent valve. Immediately prior to launch, this low pressure vent valve is closed and control of tank pressure is switched over to the primary safety relief device. At launch the liquid in the vessel is sub-cooled to the temperature corresponding to the relief-valve pressure and absorbs heat during launch and transfer to the lunar surface without the pressure rising to the point where it is necessary to vent through the relief valve. On the lunar surface, a continuous vent is opened and the vessel is continuously vented through an orifice which is sized so that the vent rate is averaged over a lunar cycle. This rate will be less than the rate required to keep the vessel pressure constant during the lunar day and greater than that required to keep the vessel pressure constant during the lunar night. Thus, the vessel pressure (and fluid temperature) will fluctuate over the lunar cycle and the fluid in the vessel will act as a thermal flywheel. The continuously venting gas can be used to intercept conductive heat

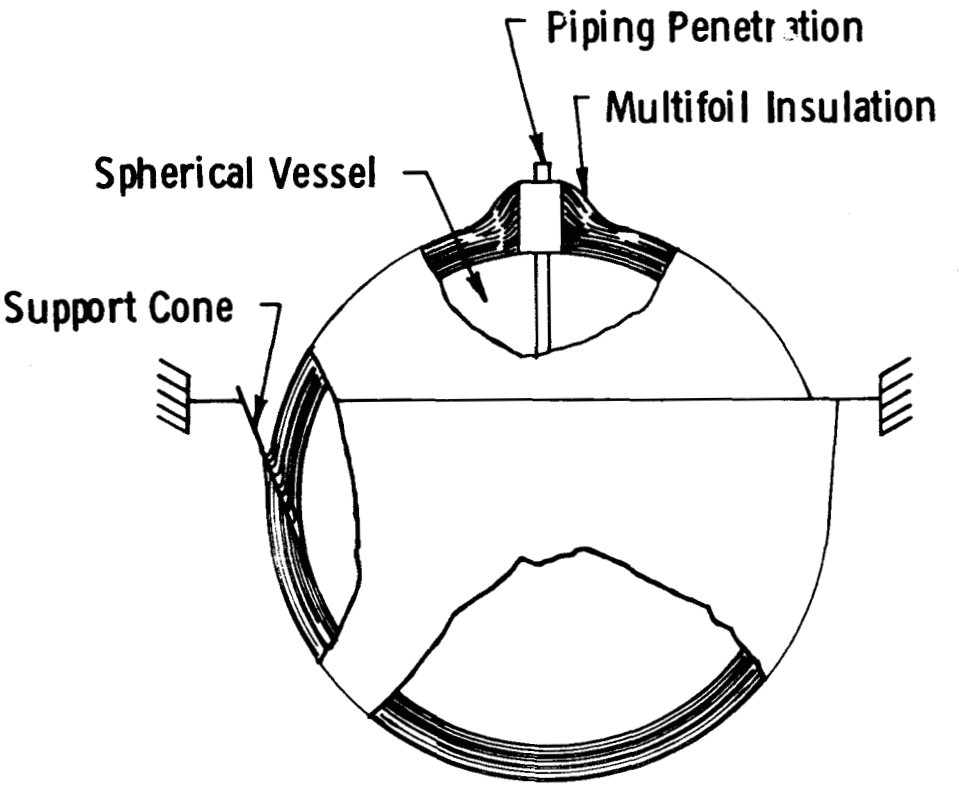

FIGURE IV-4 CONE SUPPORT FOR A CRYOGENIC VESSEL

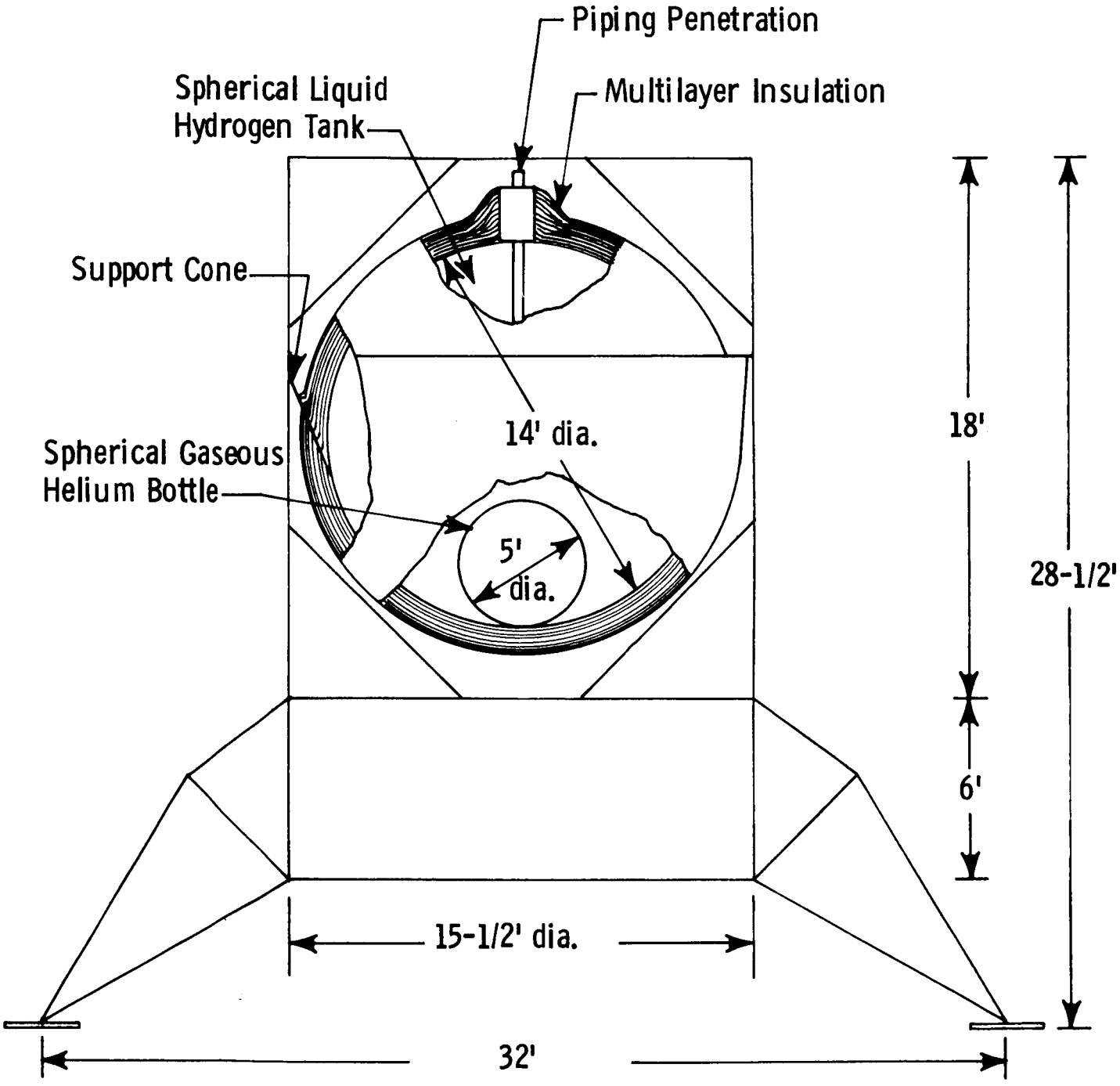

FIGURE IV-5 HYDROGEN STORAGE VESSEL CONCEPT

leaks down supports and in the pipes in the piping penetration, and for cooling of the radiation shield. To withdraw liquid on the lunar surface, the liquid withdrawal line is opened and the liquid forced out by gas pressure. Pressurized helium gas is introduced into the vessel ullage space to maintain the required pressure during this transfer.

2. Piping Penetrations

Penetrations such as supports and vent, pressurization, fill and drain lines will pass through the insulation and contact the outside warm shroud. Because of the highly anisotropic properties of multilayer insulations, imposed temperature gradients at the junction with penetrations propagate rapidly along the insulation. To prevent performance degradation, individual radiation shields have to be arranged to match temperatures along the penetration on a buffer zone inserted between the shields and the penetration (ADL, 1964). A buffer zone consists of a material which approximates the temperature distribution in the insulation. The spacer material itself can act as a buffer zone. The buffer zone prevents radiation from entering the gap caused by penetrations and prevents accidental thermal shorts between the radiation shields and the penetration.

Several pipes are required for operation of the cryogenic vessel. These include pipes which penetrate the multilayer insulation, and auxiliary valves and vents. Four lines penetrate the insulation; a fill and withdrawal line, a prelaunch vent line, a high-pressure helium line, and a vessel vent line:

a. The fill and withdrawal line is used to fill the vessel with liquid hydrogen prior to launch and to withdraw the liquid on the lunar surface. The line reaches to the bottom of the liquid hydrogen vessel and terminates in an on-off valve. This one-inch diameter line is sized so that the entire contents of the vessel may be drained by pressure transfer in an 8-hour period.

b. The prelaunch vent line serves two purposes: (1) to vent the vessel during filling and while in a ready state prior to launch, and (2) to introduce helium gas for pressurization during withdrawal of hydrogen on the lunar surface. The vent requirements determine the size of this line. During the filling and ground-hold phases, the boil-off rate will be very high as a result of the cool-down heat load and the high heat leakage through the insulation system during the helium gas purge. This vent line is sized so that it does not introduce excessive pressure drops at these high venting rates. For the model vessel, this line must be about one inch in diameter.

c. The high pressure helium line is used during withdrawal to transfer helium gas from the high pressure helium bottle in the vessel through a pressure-reducing valve into the vessel ullage space via the prelaunch vent line. The amount of high-pressure helium gas required for this purpose is rather small, so that a 1/4-inch diameter line will suffice. The high-pressure helium bottle is charged prior to launch through the helium fill line.

d. The vent line originates in the vessel ullage space and terminates in an orifice which serves as a continuous vent on the lunar surface and as a safety relief device. This line is thermally coupled to the other three lines in the piping penetration so that the continuously venting gas intercepts heat leaks down these lines during lunar storage. Since the venting rate is small, this line can be 1/4-inch diameter.

The piping penetration, located on the top center line of the tank, is shown in detail in Figure IV-6. It consists of a plastic support tube 12 inches long and 3 inches in diameter, the prelaunch vent line, fill and withdrawal line, and high-pressure helium line. There are three equally spaced high-conductivity-material discs in the penetration. The discs pass transversely through it and are thermally bonded to both the support tube and the pipes. The vessel vent line is coiled at each of these discs and bonded to it, so that a transverse isothermal surface is established at each disc. This permits the specific heat available in the vent gases to intercept conductive heat leaks down the other three pipes and to reduce the total flux into the vessel through this penetration to a value which is considerably below that which would result if there were no thermal couplings.

The ratios of the heat leak with no discs through this penetration as a function of the heat leak for a number of thermally coupled discs in it are shown below:

Number of Discs	Ratio of Heat Leaks
0	1.0
1	0.243
2	0.091
3	0.043

The ratios of the heat leaks are representative of the specific piping penetration design used and the values of venting rate, tube size, tube wall thickness, etc., in the penetrations. The tubes were chosen with a wall thickness of 0.01 inch thick titanium. The individual shields are attached to the structural support tube of the piping penetration at a point where the tube temperature matches the shield temperature.

3. Structural Support

The structural support for the vessel is shown schematically in Figure IV-7. The support is formed by a continuous cone of a mylar honeycomb material one inch thick, bonded with 0.025 inch face sheets. The entire cone is bonded to a girth ring around the vessel and a girth ring on the vehicle shroud. The slant height of this cone is 4 feet.

The support has been designed to support the inner hydrogen tank for a longitudinal acceleration in both directions of 6-1/2 g and a transverse acceleration of 1-1/2 g, and to withstand both the tensile and the buckling loads associated with these accelerations.

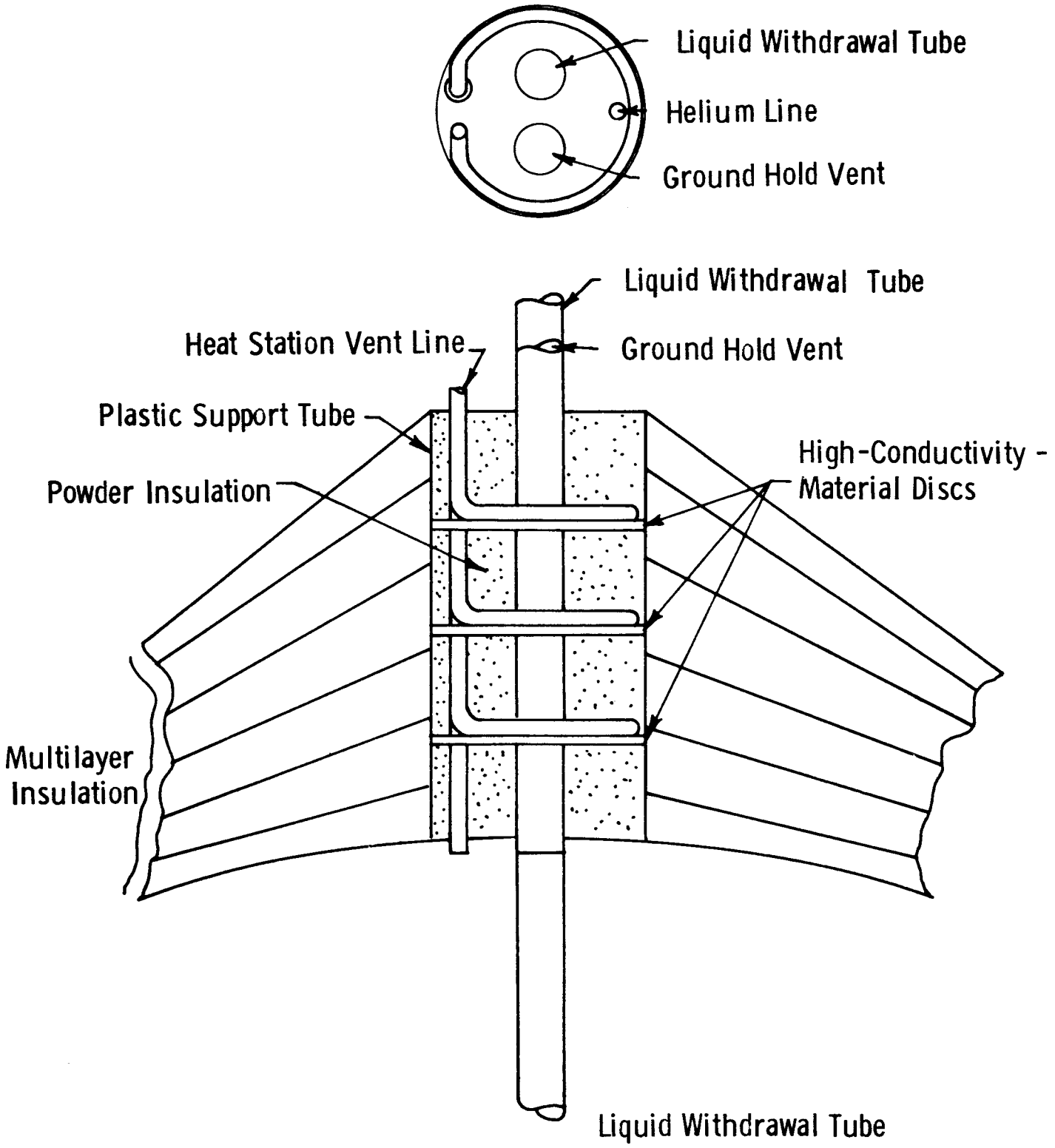

FIGURE IV-6 HYDROGEN STORAGE TANK CONCEPT--PIPING PENETRATION DETAIL

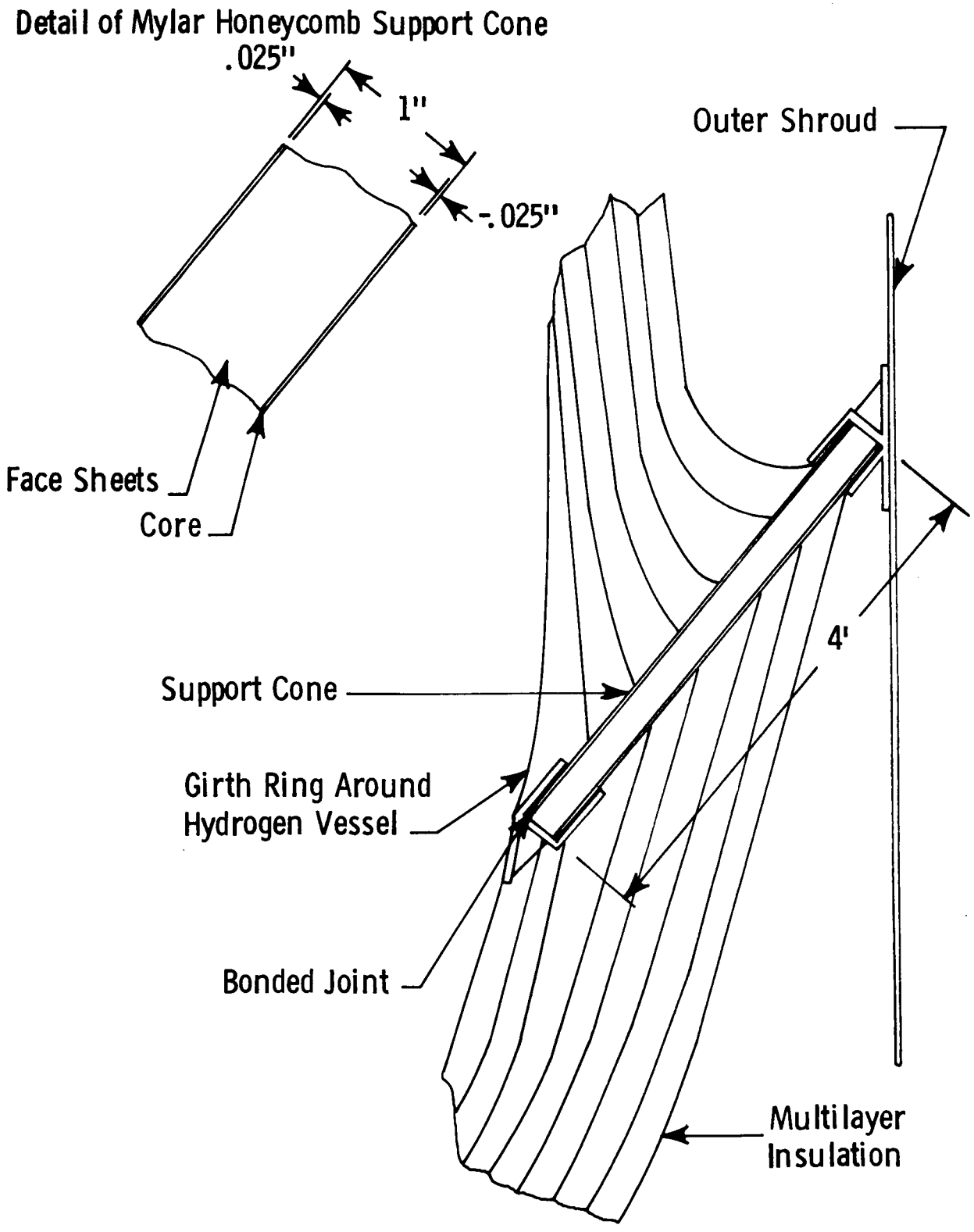

FIGURE IV-7 SUPPORT CONE DETAIL

Since this support penetrates the multilayer insulation, individual shields must be attached at locations on the cone where the temperature of the shields matches the temperature of the support cone. In this manner isothermal surfaces will be preserved around the vessel in the vicinity of the support cone, and thermal "short-circuit" will not result.

4. Outer Vessel Shroud

The outer vessel shroud is made of 1/2-inch thick aluminum honeycomb with 0.012 inch face sheets and designed to withstand axial accelerations of 6-1/2 g in both directions and transverse accelerations of 1-1/2 g. There are two support rings in the cylindrical section of the shroud, one at the point where the vessel support cone joins the shroud and another at the upper end, where the top of the cylinder joins the shroud. Additional support rings and struts may be required to carry the loads from auxiliary control equipment mounted on the top of the vessel.

V. HEAT TRANSFER ANALYSES

A. DESCRIPTION OF MATHEMATICAL MODEL

The problems of storing a cryogenic fluid on the moon have received attention in the literature (Dempster et al, 1962, Romero et al, 1956, and Buna, 1964). In addition, Arvesen and Hamaker (1964) have presented calculations of the effectiveness of radiation shields in controlling the temperatures of vehicles on the lunar surface. Dempster (1962) has calculated the heat fluxes to insulated cryogenic storage vessels in both above- and below-ground-level configurations. Buna (1964) has developed analytical techniques for predicting vaporization rates of insulated cryogenic storage tanks above the lunar surface.

Even though the lunar surface is known to conform to a photometric function which departs drastically from Lambert's cosine law, common to all of these analyses is the assumption that the lunar surface reflects sunlight diffusely in accordance with Lambert's law. Hapke (1963) has derived a photometric function which appears to conform closely with observed photometric properties of the lunar surface.

One objective of the present analysis was the computation of the heat leakage to a cryogenic storage vessel on the lunar surface for photometric functions conforming to Lambert's law and Hapke's formula. The mathematical model used in the heat leakage computations was based on the model cryogenic vessel design discussed in Section IV-D. The critical aspects of the design were treated in sufficient detail to permit realistic heat leak computations.

To carry out precise computations of the heat exchange with a storage vessel on the lunar surface it would have been necessary to design the entire vessel in detail: including, for example, the structural supports, the internal electronics and control configuration, and the various struts and support rings.

A complete structural and system analysis was outside the scope of this program; therefore, several idealizations had to be made to create a simplified mathematical model which could be used to evaluate the heat leakage to the cryogenic fluid for various characteristics of the lunar surface.

The external geometry of the simplified vessel model is shown in Figure V-1. The outer surface is a right circular cylinder with a radius of 236 centimeters and a height of 732 centimeters. The cylindrical vessel is assumed to be located 137 centimeters above the lunar surface.

To compute the heat flux incident on various zones of the outer surface, it is subdivided into 30 zones: 6 on the bottom, 6 on the top, and 18 on the side. The cylindrical surface is divided into three bands of equal height.

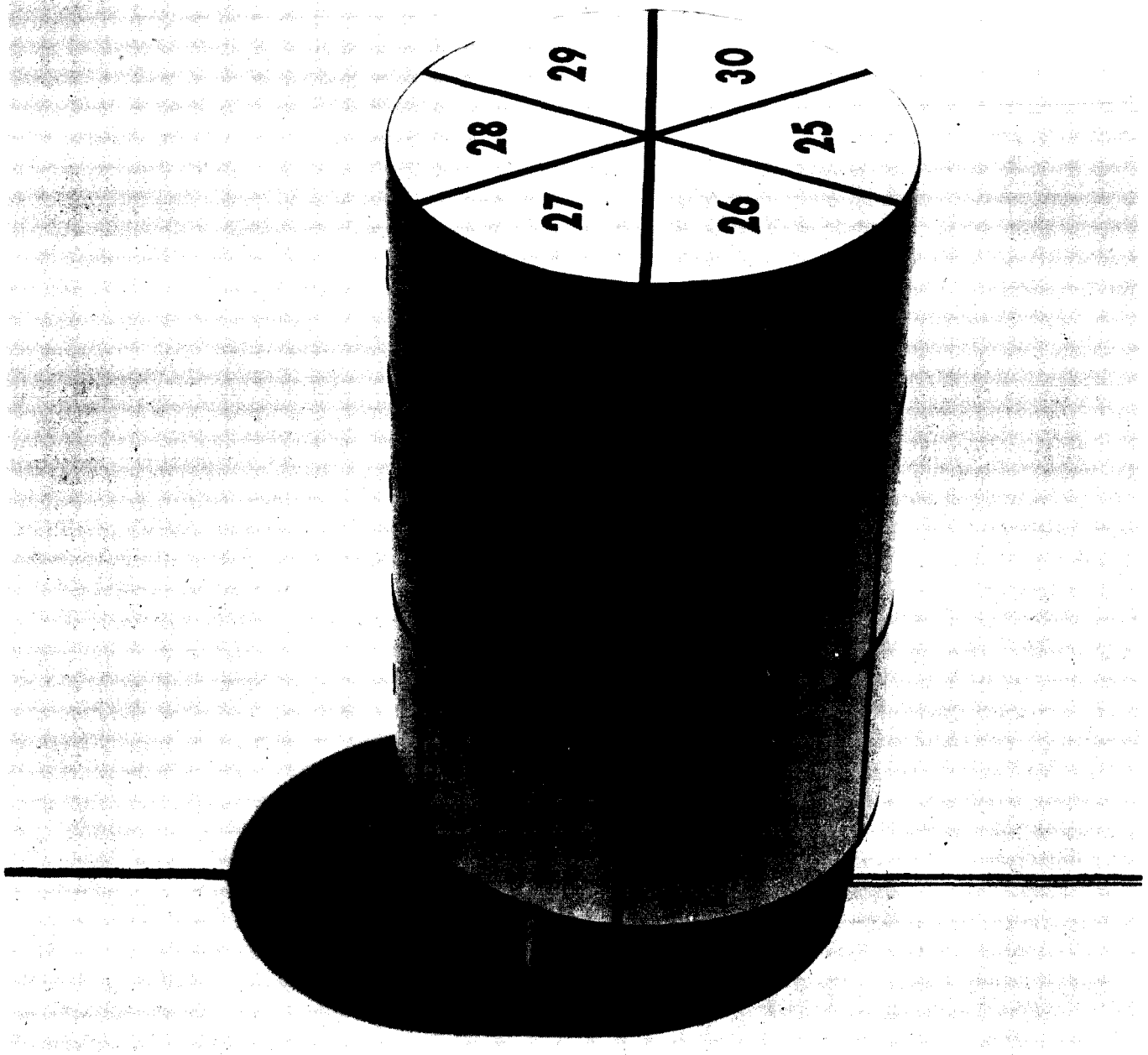

FIGURE V-1 ZONAL SUBDIVISIONS OF MODEL CRYOGENIC STORAGE VESSEL

The inner vessel contains the liquid hydrogen and is separated from the outer skin by multilayer insulation. Included in the calculations are the heat leak through the insulation and the conductive heat leaks to the inner vessel from the outer shroud. The conductive terms represent the contribution of supports and piping penetrations to the total heat transfer to the inner vessel.

In the computation of the temperatures of the external surface, the effects of the legs that would support an actual vessel were neglected. The very low thermal diffusivity of the lunar surface would cause the support legs to have a temperature distribution resulting from the radiation interchange with the lunar environment. The design and the materials of the support legs could be such that their effects on the temperature of the external surface would be very small compared to the effects of other heat inputs.

To calculate the boil-off rate of the liquid hydrogen in the storage vessel, 2440 kilograms of fluid were assumed to be stored at 20.4°K at 1 atmosphere pressure.

This mass (as discussed in Section IV-D) could be stored in a spherical vessel of 426.7 cm diameter with a 10% ullage volume and with a sphere of 152.4 cm diameter inside the vessel to store gaseous helium for pressurization.

B. ASSUMPTIONS

1. Lunar Environment

a. The storage vessel is located on the surface of the moon in the ecliptic plane and the temperature of the lunar surface is:

$$T_m = T_{ss} \sin^{1/4} el \qquad 0^o \leq el \leq 180^o$$

$$T_m = T_{min} \qquad 180^o < el < 360^o$$

where

T_m = lunar surface temperature (°K)

T_{min} = temperature of the surface during the lunar night

T_{ss} = subsolar temperature

el = sun elevation angle

The subsolar temperature is 389°K (Arvenson and Hamaker, 1964) and the values of T_{min} at various times are 122,100°K and 80°K.

b. The intensity of the direct solar radiation at the lunar surface is 0.14 watts/cm^2.

c. The infrared emittance of the lunar surface is unity.

d. When the lunar surface is assumed to obey Lambert's law, its reflectance for solar radiation is taken to be 0.07. When the lunar surface is assumed to obey Hapke's photometric function, the particle reflectivity is taken to be 0.16; in this case, the compaction parameter is taken to be 0.6. The relationship between the individual particle reflectivity and the effective hemispherical reflectance of a surface which obeys Hapke's law has not been established. The values mentioned above represent our best estimates of lunar surface conditions.

e. The lunar period is 27.32 days.

f. The temperature of the shadowed region of the lunar surface is 122°K.

2. External Vessel Surface and Shroud

a. The solar absorptance and infrared emittance of the external surface is spatially uniform and independent of temperature. In the calculations of heat leakage rates, the solar absorptance-to-emittance ratio is 0.2, 0.5, or 1.0.

b. The shroud is non-conducting and its thermal mass is negligible (see Appendix A).

c. Radiation emitted or reflected from the external shroud does not return to the surface of the shroud.

d. The external shroud is conductively de-coupled from the lunar surface.

e. Each of the thirty zones of the mathematical model of the external shroud is isothermal.

3. Insulation

a. The insulation effectiveness is characterized by a radiative shielding factor (see Appendix B), defined by the expression:

$$\mu = \frac{2n}{\epsilon_s}$$

where n = number of shields making up the multilayer insulation,

ϵ_s = emittance of the shields.

b. The heat flow through the shields is one-dimensional and the thermal mass of the insulation is negligible.

c. In heat leakage calculations to determine the influence of the shielding factor on the heat leak to the inner vessel, the shielding factor is 5000, 10,000 or 20,000. (See Appendix B for a discussion of the relationship between the number of shields, their emittance and the shielding factor.

4. Cryogen Properties

a. The inner, insulated vessel contains liquid hydrogen at a pressure of one atmosphere.

b. The temperature of the hydrogen is 20.4°K; the heat of vaporization is 107.21 cal/g (193 Btu/lb).

c. In calculating the boil-off rate of liquid hydrogen, the vaporized fraction is vented directly to the lunar environment.

d. None of the heat leakage raises the sensible enthalpy of the venting gas.

5. Structural Penetrations

a. The external shroud is conductively coupled to the inner storage vessel by twelve penetrations. Six penetrations, each having a conductance of 0.103×10^{-3} watts/°K, couple the six zones on the top of the external shroud to the inner vessel. Six other penetrations, each having a conductance of 0.427×10^{-3} watts/°K, couple the six middle zones of the cylindrical portion of the shroud to the inner vessel. The total penetration conductance was varied in the computer calculations of heat leakage. The influence of a variation in the penetration conductance on the heat leakage is discussed in Section VII.

C. CALCULATION OF INCIDENT HEAT FLUXES

We selected the following numerical method for calculating the radiative heat fluxes incident upon a cylindrical vessel supported above the lunar surface.

Ideally, it would be desirable to select a well-mapped region of the moon and base a calculation on the actual contours of this locality; however, such a procedure would be complex and beyond the scope of this program. Therefore, on a gross scale, the region around the cryogenic storage vessel (i.e., out to the horizon) is considered to be smooth; on a microscope scale, the lunar surface is considered to reflect sunlight according to either Hapke's photometric function

(Hapke, 1963) or Lambert's law. Since little is known about the emittance of the surface in the infrared (see Section C-2-c), we assume that the surface of the moon emits according to Lambert's law with an emittance of one (any surface with unit emittance must obey Lambert's law). We also assume that the surface of the cylindrical vessel obeys Lambert's law in emission and absorption. This assumption should remain valid even if the surface of the cylinder is transformed to a condition resembling the surface of the moon (e.g., by deposition of lunar particulate materials), since the infrared emittance of either type of surface is high.

The presence of the vessel will not alter the surface temperature of the moon except for part of the surface which is in the shadow cast by the vessel. The temperature in the shadow will be very low because of the poor conductivity of the surface layer on the moon.

The transition region, in which a temperature gradient exists around the edge of the shadow, is very narrow, as is the region of the penumbra; therefore, the transition is assumed to be perfectly sharp. The shape of the shadow is actually a rectangle with semicircular caps at the two opposite ends (see Figure V-1). To simplify the calculation of the view factors between zones on the vehicle and the shadow, we replace the actual shadow with a rectangle of equal area.

The basic expression to evaluate is

$$q = \int_{A_1} \int_{A_2} \frac{1}{|s|^2} \frac{dI}{d\omega} \cos \phi \, dA_1 \, dA_2 \qquad (V\text{-}1)$$

where A_1 = an area (exterior zone) (in cm^2) on the vessel,

A_2 = an area (in cm^2) on the moon,

q = the heat flux (in watts) leaving A_2 that falls on area A_1,

dA_1 = an element (in cm^2) of A_1,

dA_2 = an element (in cm^2) of A_2,

s = the vector (in cm) from dA_2 to dA_1,

$\frac{dI}{d\omega}$ = the radiation flux per unit solid angle (in watts cm^{-2} steradian^{-1}) leaving dA_2, and

ϕ = the angle between the outward normal of dA_1 and the line joining dA_1 and dA_2.

The radiation reaching the vessel from the lunar surface may be divided according to wavelength range into three components:

(1) Reflected Sunlight. In this case, Hapke (1963) states

$$\frac{dI}{d\omega} = \frac{2bI_0}{3\pi^2} \frac{\cos\epsilon \cos\beta}{\cos\epsilon + \cos\beta} (\sin\alpha + (\pi-\alpha)\cos\alpha) B(\alpha,g) \qquad (V\text{-}2)$$

where I_0 = intensity of sun's radiation (in watts cm^{-2}) in the vicinity of the moon,

b = reflectivity of a particle on the moon's surface,

ϵ = angle between the outward normal at dA_2 and the vector between dA_2 and dA_1 (s),

β = angle of incidence of the sunlight with respect to the normal at dA_2,

α = angle between the direction of the sun's rays and the vector between dA_1 and dA_2 (-s), and

g = a number called the "compaction parameter".

The function B is given by the relation

$$B(\alpha,g) = 2 - \frac{\tan\alpha}{2g}\left(1 - e^{-\frac{g}{\tan\alpha}}\right)\left(3 - e^{-\frac{g}{\tan}}\right) \quad 0 \leq \alpha \leq \frac{\pi}{2} \qquad (V\text{-}3)$$

$$B(\alpha,g) = 1, \alpha \geq \frac{\pi}{2}$$

For brevity, we may write

$$\frac{dI}{d\omega} = I_0 \, b \, h(\alpha,\beta,\epsilon)$$

where $h = \frac{2}{3\pi^2} \frac{\cos\epsilon \cos\beta}{\cos\epsilon+\cos\beta} (\sin\alpha + (\pi-\alpha)\cos\alpha) B(\alpha,g)$

(2) Infrared Radiation Emitted by the Lunar Surface. In this case we use Lambert's law and

$$\frac{dI}{d\omega} = \alpha \frac{\sigma T_m^4 \cos\epsilon}{\pi} \qquad \text{(V-4)}$$

where T_m is the temperature of the moon's surface in °K.

(3) Radiation from the Shadow of the Vessel. This radiation obeys the same law given in Equation (V-4), although a much lower temperature, T_s, must be substituted for the value T_m used for the sunlit area.

In general, the integration of Equation (V-1) has to be carried out numerically. To do this we replace the integrals by sums and the infinitesimal elements of area dA_1 and dA_2 by finite elements ΔA_{1i} and ΔA_{2j} and sum over both areas A_1 and A_2. The three integrals of interest are:

$$q_r = I_0 \, b \sum_i \sum_j h\,(\alpha,\beta,\epsilon) \frac{\cos\phi}{|s|^2} \Delta A_{1i} \Delta A_{2j} \qquad \text{(V-5)}$$

$$q_e = \sigma T_m^4 \sum_i \sum_j \frac{\cos\epsilon \cos\phi}{\pi |s|^2} \Delta A_{1i} \Delta A_{2j} \qquad \text{(V-6)}$$

$$q_s = \sigma T_s^4 \sum_i \sum_j \frac{\cos\epsilon \cos\phi}{\pi |s|^2} \Delta A_{1i} \Delta A_{2j} \qquad \text{(V-7)}$$

where q_r = reflected radiation (in watts),

q_e = radiation emitted by the sunlit area (in watts), and

q_s = radiation emitted by the shadow area (in watts).

The quantities that have been factored out of the summations in Equations (V-5 through V-7) are parameters, so it is convenient to calculate the sums without these factors. These sums are view areas and will be referred to as G_r, G_{em}, and G_{es}, respectively. Here we define a view area to be a view factor times the appropriate surface area.

The area of the moon visible to an element of area on the side of the cylindrical body of the vehicle is a semicircle, bounded by the tangent to the cylinder and the horizon. For purposes of numerical integration, this area of the moon is subdivided into a number of sectors and further subdivided in radius to produce a pattern such as that shown in Figure V-2, for example. The particular location of ΔA_{1i} determines the position of the mesh into which the moon's surface is subdivided. It is evident that the areas ΔA_{2j} increase with the square of their distance from the center. This is appropriate because these areas will be divided by $|s|^2$, the distance between the centers of the elements of area, and thus the contribution of each element to the view area will be approximately the same, except for the influence of the photometric function. To perform a simple error analysis for the integration over the surface of the moon, we let the photometric function be unity and replace $|s|^2$ with r^2, where r is the distance from the center of the mesh on the lunar surface. We find

$$\frac{dG}{dA_1} \doteq \int_{\Delta A_{2j}} \frac{dA_2}{r^2} = \int_{r_j}^{r_{j+1}} \int_{\theta_j}^{\theta_{j+1}} \frac{r\, dr\, d\theta}{r^2} = \Delta\theta \log\left(1 + \frac{\Delta r_j}{r_j}\right) \qquad \text{(V-8)}$$

where $\Delta\theta = \theta_{j+1} - \theta_j$ (a constant in our method of subdivision)

$\Delta r_j = r_{j+1} - r_j$

The integral in Equation (V-8) will be replaced by the quantity

$$\frac{\Delta G}{\Delta A_{1i}} = \frac{\Delta A_{2j}}{r_m^2} \qquad \text{(V-9)}$$

where r_m is the mean radius of the element ΔA_{2j}.

We find that

$$\frac{\Delta G}{\Delta A_{1i}} = \frac{\Delta\theta\, \Delta r_j}{r_j\left(1 + \frac{\Delta r_j}{2 r_j}\right)} \qquad \text{(V-10)}$$

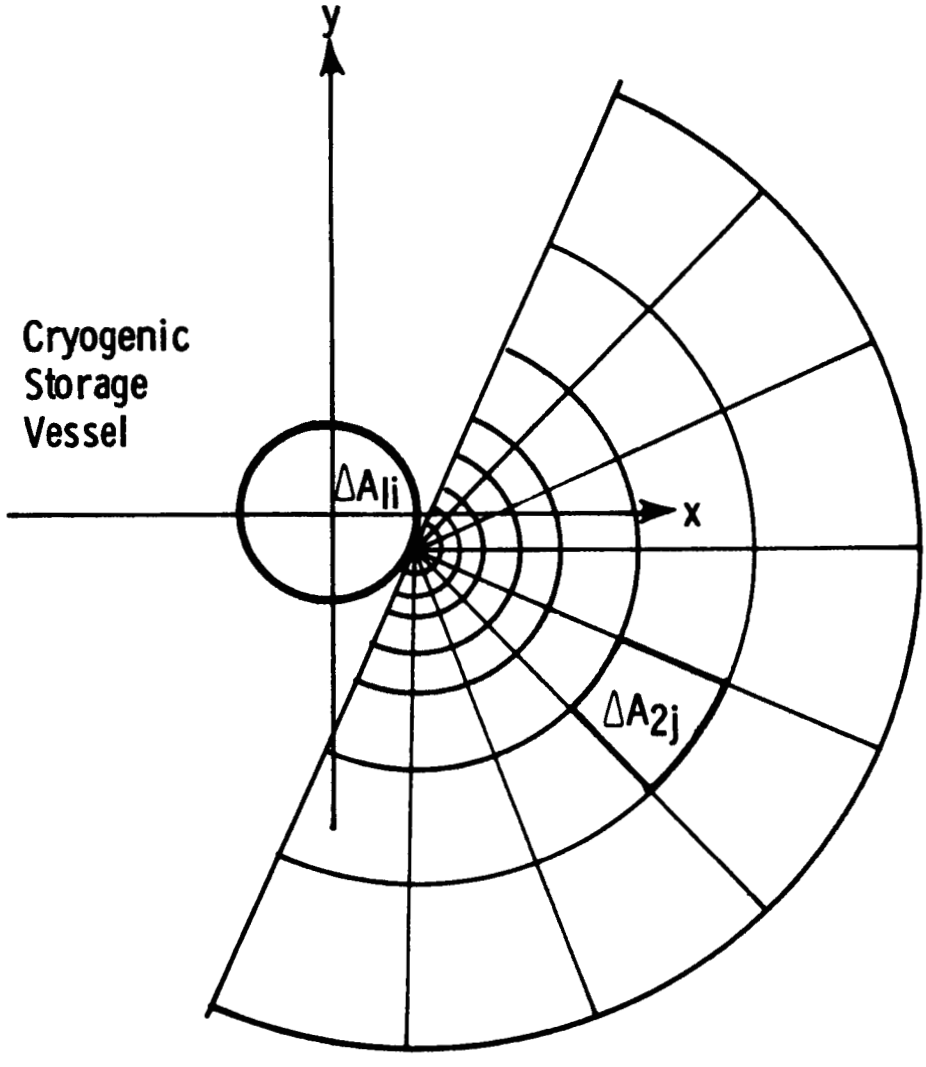

FIGURE V-2 SUBDIVISION OF THE SURFACE OF THE MOON

To estimate the error, we expand the right-hand sides of Equations (V-8) and (V-10) into power series, subtract, and select the first term that is different from zero. We find the error, η, to be given by the expression

$$\eta = \frac{\Delta \theta}{12}\left(\frac{\Delta r_j}{r_j}\right)^3 \qquad \text{(V-11)}$$

Therefore, to keep the error contribution from each element approximately the same, the quantity

$$\frac{r_{j+1}}{r_j}$$

should be held constant. The value of this constant is determined in such a way that the elements ΔA_{2j} are "square" in the sense that

$$\Delta r_j = r_m \Delta \theta \qquad \text{(V-12)}$$

It follows from Equation (V-12) that

$$\frac{r_{j+1}}{r_j} = \frac{2 + \Delta \theta}{2 - \Delta \theta} \qquad \text{(V-13)}$$

In the example shown in Figure V-2, $\Delta \theta = \frac{\pi}{8}$ and the corresponding ratio r_{j+1}/r_j is about 1.5. Then if, for example, the radius of the innermost arc is 1 meter, and the element on the cylinder is 10 meters high (which implies that the horizon is at a radius of about 6000 meters), about 22 increments of radius will be used. Thus 176 subdivisions of the visible area of the moon would be required in this case, which would result in an error of about 1% with respect to the integration over the lunar surface.

In case the area A_1 is not on the side of the vessel but is on the bottom, a similar subdivision system is employed for the surface of the moon. The only difference is that the area of the moon viewed from the underside of the vessel is a full circle instead of a semicircle.

To define vector s it is necessary to pick definite "center" points on the finite elements of area $\triangle A_{1i}$ and $\triangle A_{2j}$. These points are picked to lie midway between the boundaries of the elements, so that on the element $\triangle A_{2j}$ the mean angle and radius is used. Let (x_1, y_1, z_1) and (x_2, y_2, z_2) be the coordinates of the centers of the elements $\triangle A_{1i}$ and $\triangle A_{2j}$, respectively, and let r_m, ϕ_m be the polar coordinates of (x_2, y_2) referred to the polar system of coordinates with origin at (x_1, y_1). Then it can be shown that

$$x_2 = x_1 + r_m\left(\frac{x_1}{r_1}\sin\phi_m + \frac{y_1}{r_1}\cos\phi_m\right) \qquad \text{(V-14)}$$

$$y_2 = y_1 + r_m\left(\frac{y_1}{r_1}\sin\phi_m - \frac{x_1}{r_1}\cos\phi_m\right) \qquad \text{(V-15)}$$

where $r_1 = \sqrt{x_1^2 + y_1^2}$.

The variation of z_2 with x_2 and y_2 is small and is given by

$$z_2 = -\frac{(x_2^2 + y_2^2)}{2R} \qquad \text{(V-16)}$$

where R = radius (in cm) of the moon.

Equation (V-16) is an approximation based on the fact that the diameter of the moon is extremely large in comparison with the size of any vessel.

It is not convenient to attempt to describe the rectangular shadow in the polar coordinate system shown in Figure V-2. Therefore, the calculation of the view areas G_r and G_e (for reflection and emission) is made by first integrating over the entire visible area of the moon and then subtracting the contribution of the shadow.

The vessel's shadow, approximated by a rectangle, and the method of its subdivision are illustrated in Figure V-3. To make the shadow have the proper area, the lengths ℓ_1 and ℓ_2 are chosen to be

$$\ell_1 = \frac{h_1}{\tan\beta_s} + \frac{\pi\, r_c}{4} \qquad \text{(V-17)}$$

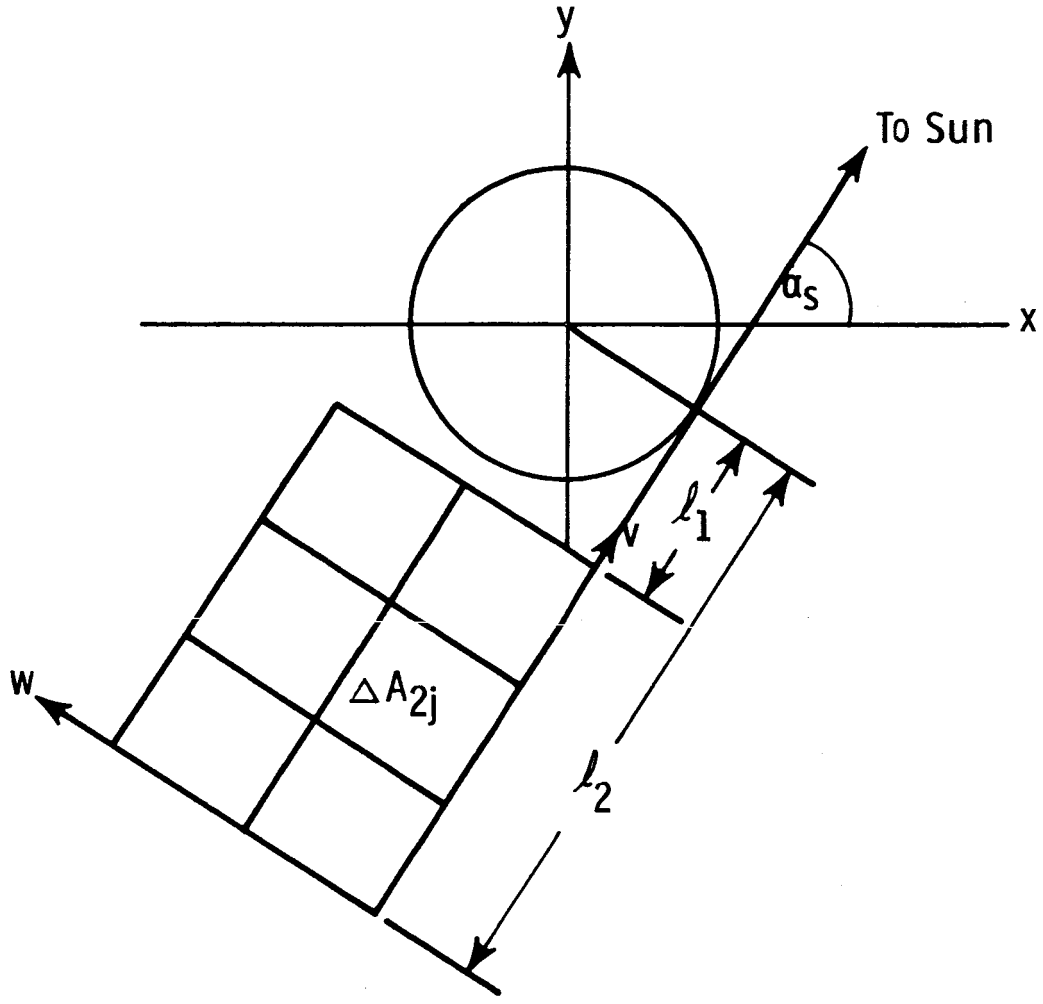

FIGURE V-3 SUBDIVISION OF RECTANGULAR SHADOW

$$\ell_2 = \frac{h_2}{\tan\beta_s} - \frac{\pi\, r_c}{4} \qquad \text{(V-18)}$$

where r_c = radius (in cm) of cylinder,

β_s = elevation angle of sun,

h_1 = height (in cm) of bottom of cylinder, and

h_2 = height (in cm) of top of cylinder.

The width of the shadow is $2r_c$.

To find the coordinates (x_2, y_2) of the center of an element ΔA_{2j} of the shadow, it is convenient to introduce first the coordinate system (v, w) as shown in Figure V-3. The origin of this system is at

$$x = r_c \sin\alpha_s - \ell_2 \cos\alpha_s \qquad \text{(V-19)}$$

$$y = -r_c \cos\alpha_x - \ell_2 \sin\alpha_s \qquad \text{(V-20)}$$

where α_s = azimuth angle of the sun. Thus, if the coordinates of the center of an element are (v_m, w_m) in the (v, w) system, the coordinates in the (x, y) system are given by

$$x_2 = v_m \cos\alpha_s - w_m \sin\alpha_s + r_c \sin\alpha_s - \ell_2 \cos\alpha_s \qquad \text{(V-21)}$$

$$y_2 = v_m \sin\alpha_s + w_m \cos\alpha_s - r_c \cos\alpha_s - \ell_2 \sin\alpha_s \qquad \text{(V-22)}$$

The coordinate z_2 is given again by Equation (V-16).

In Figure V-4 are shown the angles, α, β, ϵ, and ϕ along with the outward unit normal vector, $\hat{m}$, to the surface of the moon, the outward

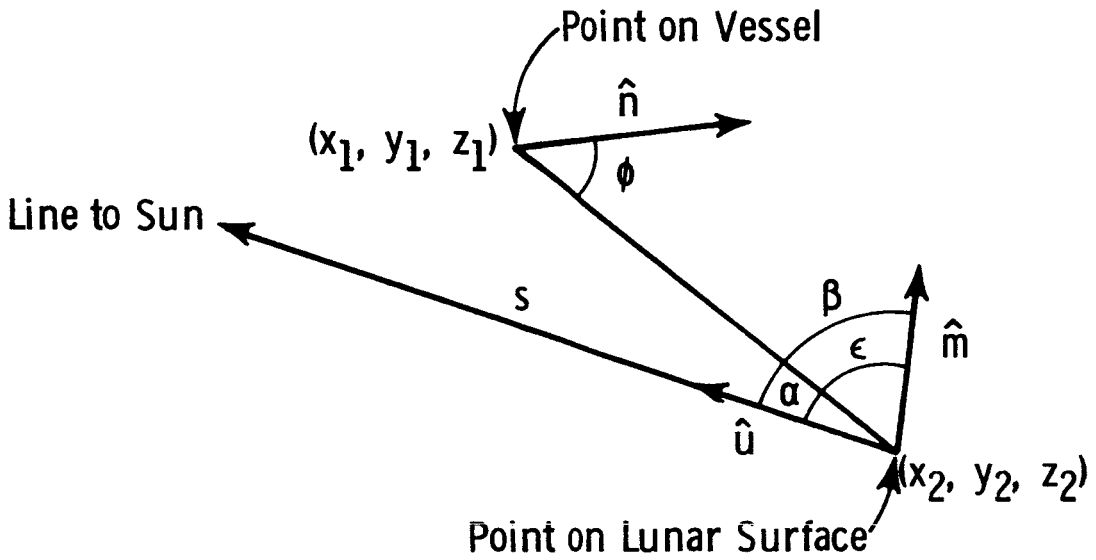

FIGURE V-4 GEOMETRICAL RELATIONSHIP OF THE SUN, A POINT ON THE VESSEL, AND A POINT ON THE LUNAR SURFACE

unit normal vector, $\hat{n}$, to the surface of the vessel and the unit vector, $\hat{u}$, directed from the point on the moon towards the sun. In terms of these vectors,

$$\cos\alpha = \frac{\hat{u}\cdot s}{|s|} \tag{V-23}$$

$$\cos\epsilon = \frac{\hat{m}\cdot s}{|s|} \tag{V-24}$$

$$\cos\phi = -\frac{\hat{n}\cdot s}{|s|} \tag{V-25}$$

where
$$s = (x_1 - x_2,\ y_1 - y_2,\ z_1 - z_2) \tag{V-26}$$

$$\hat{u} = (\cos\alpha_s \cos\beta_s,\ \sin\alpha_s \cos\beta_s,\ \sin\beta_s) \tag{V-27}$$

and the vector $\hat{n}$ may have one of two values, depending on whether ΔA_{1i} is on the side or the bottom of the vessel. On the side

$$\hat{n} = \left(\frac{x_1}{r_c},\ \frac{y_1}{r_c},\ 0\right) \tag{V-28a}$$

On the bottom

$$\hat{n} = (0,\ 0,\ -1) \tag{V-28b}$$

To a sufficient degree of approximation we may take

$$\beta = \frac{\pi}{2} - \beta_s \tag{V-29}$$

since the vector $\hat{m}$ is everywhere directed very nearly parallel to the z-axis. To the same degree of approximation we find

$$\cos\epsilon = \frac{z_1 + z_2}{|s|} \tag{V-30}$$

In connection with Equation (V-30), note that the horizon occurs at a distance

$$H = \sqrt{2Rz_1}$$

and at this distance $z_1 = - z_2$, so that both terms in the numerator of Equation (V-30) must be retained in spite of the small curvature of the lunar surface, which may be neglected elsewhere in the problem.

The numerical methods described above were employed to calculate heat fluxes from the lunar surface and incident on the surface of the cylindrical vessel. These formulas were incorporated into a computer program to calculate the fluxes in specific instances.

D. THE RESPONSE OF THE LUNAR SURFACE TO SHADOWS FROM A NEARBY OBJECT

To evaluate the heat fluxes incident upon an object which is resting on the lunar surface in sunlight, it is necessary to determine the amount of heat which comes from the lunar surface. The presence of an object resting on the lunar surface will cause a part of the surface very near the object to be shadowed (see Figure V-5). The temperature distribution in the shadow is derived below.

Consider the moon to be a semi-infinite solid bounded by the x-y plane and assume the solid to be homogeneous and to have a conductivity K and a black surface. Furthermore, let the incident illumination be S, where

$$\left.\begin{aligned} S &= 0 \quad \text{for } |x| < \ell \\ S &= S_o \quad \text{for } |x| > \ell \end{aligned}\right\} \tag{V-31}$$

Thus, the shadow will be an infinite strip of width 2ℓ along the y-axis.

The temperature in the medium, T, is determined by

$$\frac{\partial^2 T}{\partial x^2} + \frac{\partial^2 T}{\partial z^2} = 0 \tag{V-32}$$

with the boundary conditions

$$K \frac{\partial T}{\partial z} = \sigma T^4 - S \quad \text{for } z = 0 \tag{V-33}$$

$$T = T_o < \infty \quad \text{for } z = \infty \tag{V-34}$$

As they are written, Equations (V-32) through (V-34) are completely intractable because of the nonlinearity of the boundary condition (V-33). To obtain approximate results, we will write the equations in terms of $u = \sigma T^4$ and drop nonlinear terms. We find

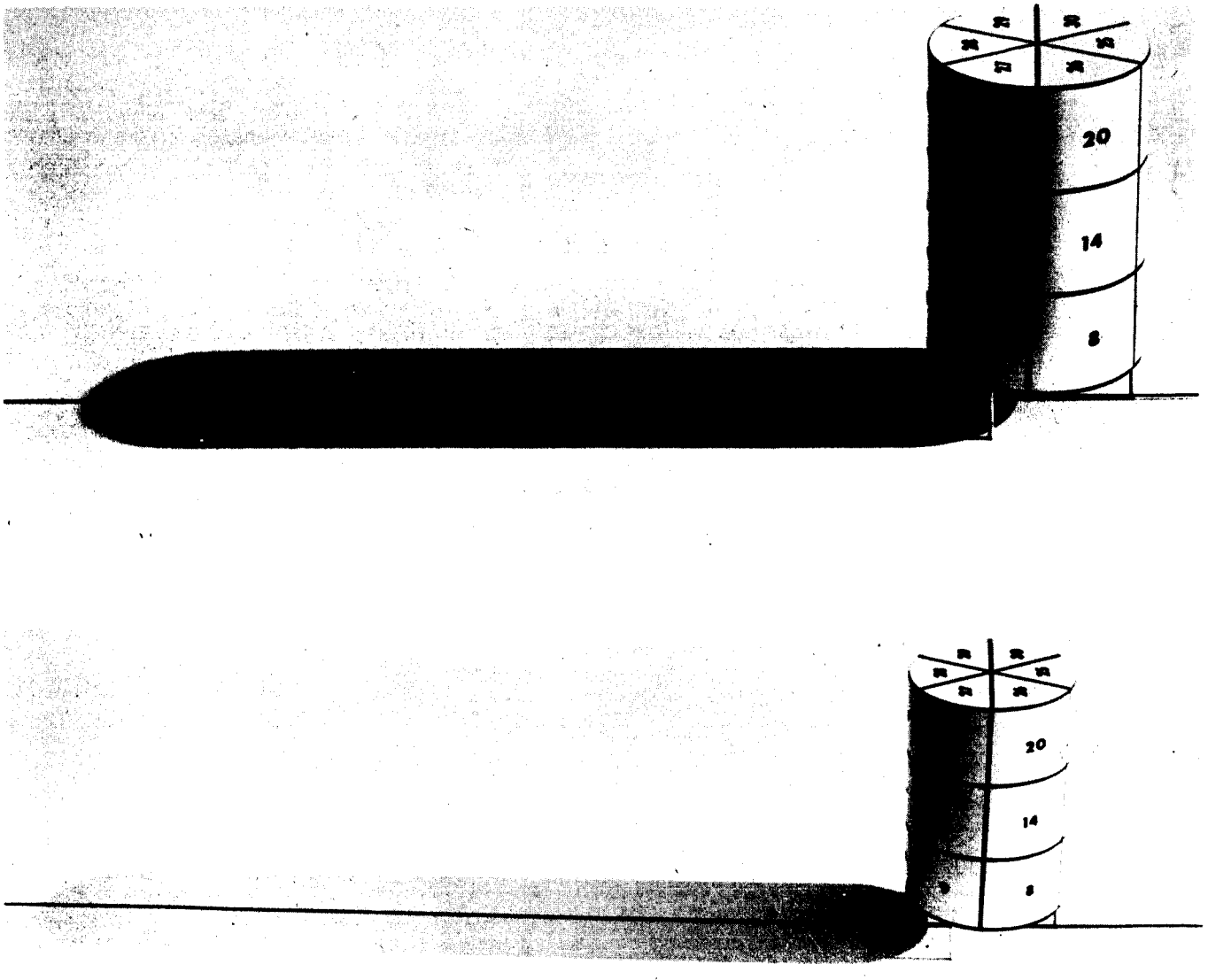

FIGURE V-5 FORMATION OF SHADOWS ON THE LUNAR SURFACE BY A VESSEL

$$\frac{\partial^2 u}{\partial x^2} + \frac{\partial^2 u}{\partial z^2} = 0 \qquad \text{(V-35)}$$

$$\frac{K}{4\sigma T_o^3} \frac{\partial u}{\partial z} = u - S \qquad \text{for } z = 0 \qquad \text{(V-36)}$$

$$u = u_o < \infty \quad \text{for } z = \infty \qquad \text{(V-37)}$$

Here we have arbitrarily linearized about T_o.

We now employ Fourier transforms to obtain a more useful expression for S. We find

$$S = S_o \left(1 - \frac{2}{\pi} \int_0^\infty \frac{\sin k\ell \cos kx}{k} dk\right) \qquad \text{(V-38)}$$

We may also write

$$u = \int_0^\infty \phi(k) \cos kx e^{-kz} dk + u_o \qquad \text{(V-39)}$$

where $\phi(k)$ is to be determined by the boundary condition (V-36) and $u_o = \sigma T_o^4$. As defined by Equation (V-39), the function u satisfies the differential equation (V-35) and meets the boundary condition (V-37) at $z = \infty$. To find $\phi(k)$ explicitly, we substitute Equation (V-39) into Equation (V-36) to obtain

$$-\frac{K}{4\sigma T_o^3} \int_0^\infty k\phi(k) \cos kx\, dk = \int_0^\infty \phi(k) \cos kx\, dk + u_o - S_o + \frac{2S_o}{\pi} \int_0^\infty \frac{\sin k\ell \cos kx}{k} dk \qquad \text{(V-40)}$$

If we let $u_o = S_o$ and make use of the fact that Equation (V-40) must be satisfied for all values of x, we find that

$$\phi(k) = - \frac{2 \sin k\ell}{\pi k \left(1 + \frac{K k}{4\sigma T_o^3}\right)} u_o \qquad \text{(V-41)}$$

Equation (V-41) may now be substituted into Equation (V-39) to give the formal solution

$$u = u_o \left\{1 - \frac{2}{\pi} \int_0^\infty \frac{\sin k\ell \cos kx \, e^{-kz}}{k \left(1 + \frac{K k}{4\sigma T_o^3}\right)} dk \right\} \qquad \text{(V-42)}$$

We are only concerned here with the surface temperature, T_s, which we may find from Equation (V-42) by setting $z = 0$. We obtain

$$u_s = u_o \left\{1 - \frac{2}{\pi} \int_0^\infty \frac{\sin k\ell \cos kx}{k \left(1 + \frac{K k}{4\sigma T_o^3}\right)} dk \right\} \qquad \text{(V-43)}$$

where $$u_s = \sigma T_s^4 \qquad \text{(V-44)}$$

The integral appearing in Equation (V-43) can be evaluated in terms of the sine and cosine integral functions. We find

$$u_s = \frac{u_o}{\pi} \left\{ f(\xi_1) + f(\xi_2) \right\} \qquad \text{for } 0 \leq x \leq \ell \qquad \text{(V-45a)}$$

$$u_s = u_o - \frac{u_o}{\pi} \left\{ f(|\xi_1|) - f(\xi_2) \right\} \qquad \text{for } x \geq \ell \qquad \text{(V-45b)}$$

where

$$\xi_1 = \frac{4\sigma T_o^3 (\ell - x)}{K} \qquad \text{(V-46)}$$

$$\xi_2 = \frac{4\sigma T_o^3 (\ell + x)}{K} \qquad \text{(V-47)}$$

$$f(\xi) = Ci(\xi)\ \sin\xi + \left[\frac{\pi}{2} - Si(\xi)\right]\ \cos\xi \qquad \text{(V-48)}$$

For our purposes a reasonable approximation to $f(\xi)$ may be used to advantage. It may be shown that

$$f(\xi) = \frac{1}{\xi + \frac{2}{\pi}} \quad \text{for } 0 \leq \xi < \infty \qquad \text{(V-49)}$$

Thus we find

$$u_s = u_o \left\{ \frac{1}{2 + \frac{\ell - x}{\lambda}} + \frac{1}{2 + \frac{\ell + x}{\lambda}} \right\}, \quad 0 \leq x \leq \ell \qquad \text{(V-50a)}$$

$$u_s = u_o \left\{ 1 - \frac{1}{2 + \frac{x - \ell}{\lambda}} + \frac{1}{2 + \frac{\ell + x}{\lambda}} \right\}, \quad x \geq \ell \qquad \text{(V-50b)}$$

where λ is a characteristic length given by the expression

$$\lambda = \frac{K}{4\pi\sigma T_o^{\,3}} \qquad \text{(V-51)}$$

We may take the following values as representative of what may be expected on the lunar surface

$K = 10^{-3}$ watts cm^{-1} $(deg\ K)^{-1}$ (for vesicular materials, such as pumice in a vacuum)

$T_o = 350^{\circ}K$

Using these values, we find

$$\lambda = 0.3 \text{ cm.}$$

If we take the width of the shadow to be 200 cm, the last terms in Equations (V-50a) and (V-50b) are completely negligible and we find that the width of the region about the edge of the shadow in which any appreciable temperature gradient exists must at most be of the order of 2 centimeters. Should the lunar surface be covered with a dust layer, the conductivity, K, and hence the characteristic length, λ, will be two orders of magnitude smaller.

We conclude, therefore, that in calculating the heat flux incident upon a storage vessel which casts a shadow on the lunar surface, we can safely ignore the region about the edge of the shadow in which a temperature gradient exists. Thus, a single temperature can be assigned to the shadow areas and a single temperature can be assigned to the sunlit areas for purposes of heat flux calculations.

We may next estimate the time the lunar surface takes to cool off after the object casting the shadow is emplaced. If we assume Newton's law of cooling to prevail, which amounts to linearizing the radiation boundary condition, we find (Carslaw and Jaeger, 1959) that

$$T \doteq \frac{KT_o}{h\sqrt{\pi\ \kappa\ t}} \qquad \text{(V-52)}$$

where T = temperature (in ^oK) of surface,

T_o = initial temperature (in ^oK),

K = thermal conductivity (in watts cm^{-1} $(^oK)^{-1}$),

h = heat transfer coefficient (in watts cm^{-2} $(^oK)^{-1}$),

κ = thermal diffusivity (in cm^2 sec^{-1}), and

t = time (in sec).

Equation (V-52) may be solved for the time t to yield

$$t = \frac{1}{\pi}\left(\frac{T_o}{h\gamma T}\right)^2 \qquad \text{(V-53)}$$

where the thermal parameter γ is given by

γ = $(K\ \rho\ C)^{-1/2}$ (in $joules^{-1}$ cm^2 $sec^{1/2}$ ^oK),

ρ = density (in gm cm^{-3}),

C = heat capacity (in joules gm^{-1} $(^oK)^{-1}$).

We may take

T_o = 370^oK

T = 200^oK

γ = 250 $joules^{-1}$ cm^2 $sec^{1/2}$ ^oK

h = $4\sigma T^3$ = 1.8×10^{-4} watts cm^{-2} $(^oK)^{-1}$

and we find $t = 540$ sec.

This is a maximum estimate of the time required for the radiation emitted in the shadowed area to fall to one-tenth of its initial value. We may conclude, therefore, that the shadowed area will cool down to a low temperature immediately after the shadow falls. The temperature of the shadow thus need not be considered to be time dependent.

E. HEAT FLOW EQUATIONS

Using the methods previously described in Section V-3, we calculated the heat leakage to the inner insulated cryogenic storage vessel resulting from the heat flux incident on the external shroud. Assuming that the shroud was adiabatic in that no heat flux due to azimuthal conductance or conductance normal to the shroud was assumed to exist and had a negligible thermal mass (see Appendixes A and C), we calculated the steady state temperatures of each zone of the external shroud.

The temperature of each zone (assumed to be isothermal) was calculated from the heat balance equation:

surface moon shadow sun albedo

$$\epsilon_s A_z \sigma T^4 = \epsilon_s G_{em} \sigma T_m^4 + \epsilon_s G_{es} \sigma T_{ms}^4 + \alpha_s I_o G_s + \alpha_s q_r \qquad \text{(V-54)}$$

where q_r = heat flux (in watts) due to reflection, which is calculated according to the equations:

$bI_o G_r$ (for a Hapke reflector) and

$aI_o G_{em}$ (for a Lambert reflector),

α_s = solar absorptance of the skin of the vessel,

ϵ_s = infrared emittance of the skin of the vessel,

T = mean temperature of a zone,

T_m = temperature (in ^oK) of the sunlit lunar surface,

T_{ms} = temperature (in ^oK) of the shadow on the lunar surface,

σ = Stefan-Boltzmann constant = 5.6686×10^{-12} watts/cm^2 $(^oK)^4$,

I_o = intensity of solar radiation - 0.14 watts/cm^2,

a = lunar surface albedo fraction,

b = particle reflectivity of the lunar surface.

A_z = area of the zone (cm^2)

G_s = view area (in cm^2) of the zone to the sun

G_{em} = view area for sunlit part of lunar surface

G_{es} = view area for shadowed part of lunar surface

Note that Equation (V-54) can be written in the form

$$A_z \sigma T^4 = G_{em} \sigma T_m^4 + G_{es} \sigma T_{ms}^4 + \frac{\alpha_s}{\epsilon_s} (I_o G_s + q_r) \qquad \text{(V-55)}$$

Thus, the temperature of each shroud zone is independent of the magnitudes of the emittance and solar absorptance and only depends on the solar absorptance-to-emittance ratio.

The heat flux into the liquid hydrogen storage vessel at a given time is calculated from the formula:

$$q\,(el) = \sum_{i=1}^{30} \left[\frac{A_{z(i)}}{\mu} \left(\sigma\, T^4\,(i,el) - \sigma\, T_{H_2}^4 \right) + C_{(i)} \left(T\,(i,el) - T_{H_2} \right) \right] \qquad \text{(V-56)}$$

where q(el) = heat flux (in watts) into the LH_2 storage vessel at a given sun elevation angle,

Az(i) = area (in cm^2) of zone number i,

μ = the shielding factor for the insulation separating the inner LH_2 storage vessel from the external shroud,

T (i,el) = mean temperature (in ^oK) of zone i at a given sun elevation angle,

C(i) = penetration conductance (in watts/^oK) into zone i, and

T_{H_2} = temperature of liquid hydrogen (assumed to be 20.4^oK).

The average flux into the tank over a lunar day, $\bar{q}$, is found by integrating q(el) by the trapezoidal rule. The per cent boil-off of liquid hydrogen per year is given by

$$B = \frac{Q}{m\, h_{fg}} \times 100 \qquad \text{(V-57)}$$

- B = boil-off rate (in %) per year,
- Q = total heat influx (in watts) to the cryogen in a one-year period,
- m = initial mass (in kg) of stored hydrogen,
- h_{fg} = heat of vaporization (in watts sec kg^{-1}) of the liquid hydrogen.

VI. COMPUTER PROGRAMS

We prepared three programs to calculate the average yearly boil-off rate of liquid hydrogen from a storage vessel on the surface of the moon.

A. VIEW AREAS

The first program of the set, written FORTRAN II for the IBM 7090, is used to calculate three view areas for a portion (to be referred to as a zone) of the cylindrical vessel:

1. from the zone to the unshadowed region of the lunar surface (for emission and for reflection),
2. from the zone to the shadow of the vessel on the lunar surface, and
3. from the zone to the sun.

Since the sun is considered to be a source of plane waves, the view area of a zone of the vessel to the sun is the area of the zone projected onto a plane perpendicular to the sun line. This view area is then defined by the integral:

$$G_s = \int_{A_z} \hat{u} \cdot \hat{n} \, dA_z \qquad \text{(VI-1)}$$

where G_s = view area (in cm^2) of the zone to the sun,

A_z = area (in cm^2) of the zone,

$\hat{u}$ = unit vector from a point on the vessel to the sun (i.e., the same as taking a unit vector from a point on the lunar surface to the sun),

$\hat{n}$ = outward unit normal to the surface of the vessel.

The view area of a zone on the vessel to the unshadowed lunar surface to be used for reflection was found by Hapke (1963) to be:

$$G_r = -\int_{A_m}\int_{A_z} h(\alpha, \beta, \epsilon) \frac{\vec{s} \cdot \hat{n}}{|\vec{s}|^3} \, dA_z \, dA_m \qquad \text{(VI-2)}$$

where G_r = view area (in cm^2) of the zone to the unshadowed lunar surface to be used in calculating flux due to reflection,

s = vector (in cm) directed from a point on the lunar surface to a point on the vessel,

A_m = area (in cm^2) of the unshadowed lunar surface,

$h(\alpha,\beta,\epsilon)$ = (as defined in Section V),

$$\alpha = \cos^{-1}\left(\frac{\vec{s} \cdot \hat{u}}{\vec{s}}\right),$$

$$\beta = \cos^{-1}(\hat{u} \cdot \hat{m}),$$

$$\epsilon = \cos^{-1}\left(\frac{\hat{m} \cdot \vec{s}}{|s|}\right),$$

$\hat{m}$ = outward unit normal to the lunar surface.

The view area of a zone on the vessel to the unshadowed lunar surface to be used in calculating flux due to emission may be determined from Lambert's law:

$$G_{em} = -\frac{1}{\pi}\int_{A_m}\int_{A_z}\frac{(\hat{m} \cdot \vec{s})(\vec{s} \cdot \hat{n})}{|\vec{s}|^4}\, dA_z\, dA_m \qquad \text{(VI-3)}$$

Similarly, the view area of a zone on the vessel to the shadow of the vessel is

$$G_{es} = -\frac{1}{\pi}\int_{A_s}\int_{A_z}\frac{(\hat{m} \cdot \vec{s})(\vec{s} \cdot \hat{n})}{|\vec{s}|^4}\, dA_z\, dA_s \qquad \text{(VI-4)}$$

where G_{em} = view area (in cm^2) of a zone to the unshadowed lunar surface to be used for emission,

G_{es} = view area (in cm^2) of a zone to the shadow of the vessel to be used for emission, and

A_s = area (in cm^2) of the shadow of the vessel.

The view area program requires as input data the azimuth and elevation of the sun, the radius and height of the cylindrical vessel, the distance that the vessel stands above the lunar surface, the compaction parameter, a description of the zone on the vessel, and the mesh to be used in the numerical integration of G_s, G_r, G_{em}, G_{es}. These data are given on a set of 5 cards in the FORTRAN format:

I5,6F10.5,I5

This set of cards must be followed by a blank. The data on the cards are:

I5	F10.5	F10.5	F10.5	F10.5	F10.5	F10.5	I5
1	as	el					
2	nt_m	mr					
3	r_c	z_1	z_2	ds			n job
*4	d_1	d_2	n_d	t_1	t_2	nt	n zone
*5	d_1	d_2	n_d	t_1	t_2	nt	n zone
6	g						

* Only one of these cards is used in a data set.

where Card 1--Information on the position of the sun

as = azimuth angle (in degrees) of the sun,

el = elevation angle (in degrees) of the sun.

(Note that el must not be zero, because the program will not properly handle an infinitely long shadow which begins an infinite distance from the vessel.)

Card 2--Information for integration over the lunar surface

nt_m = number of divisions to use per 180^o, and

mr = mean radius (in cm) of the first radial subdivision.

Card 3--Description of the cylindrical vessel

r_c = radius (in cm) of the cylinder,

z_1 = distance (in cm) of the bottom of the vessel from the lunar surface,

z_2 = distance (in cm) of the top of the vessel from the lunar surface,

ds = approximate mesh size (in cm) to be used in integrating over the shadow,

n job = job number.

Card 4--Description of a zone on side of the cylinder

d_1, d_2 = z limits (in cm) of the zone,

nd = number of subdivisions to take in integrating in the z dimension,

t_1, t_2 = θ limits (in degrees) of the zone,

nt = number of subdivisions to take in integrating in the θ dimension,

n zone = zone number.

Card 5--Description of zone on bottom of the cylinder

d_1, d_2 = r limits (in cm) of the zone,

nd = number of subdivisions to take in integrating in the r dimension,

t_1, t_2, nt = n zone as in card 4.

Card 6--Additional information

g = compaction parameter of the lunar surface to be used in Hapke's formula.

The caid output from the view area program for each zone is a set of three cards in the FORTRAN format:

3I5,4E15.8

which contain the information:

I5	I5	I5	E15.8	E15.8	E15.8	E15.8
1	n job	n zone	a_s(radians)	el(radians)	G_s	
2	n job	n zone	a_s(radians)	el(radians)	G_{em}	G_{es}
3	n job	n zone	a_s(radians)	el(radians)	G_r	G_{rs}

where

$$G_{rs} = -\int_{A_s}\int_{A_z} h\,(\alpha, \beta, \epsilon)\,\frac{\vec{s}\cdot\hat{n}}{|s|^3}\,dA_z\,dA_m \qquad \text{(VI-5)}$$

which is calculated for checking purposes. The printed output consists of the input data with the notation as given above. Following the zone number is printed a C if the zone is on the side of the cylinder and a D if the zone is on the disc, i.e., the bottom of the vessel. The view areas are printed with the following notation:

incident sun $\equiv G_s$

Lambert - moon $\equiv G_{em}$

Lambert - shadow $\equiv G_{es}$

Hapke - moon $\equiv G_r$

Hapke - shadow $\equiv G_{rs}$

The remaining two programsof the set of three were written for the specific case of a vessel on the lunar ecliptic. The vessel has been divided into 30 zones, of which 6 are on the bottom and 6 are on the top of the vehicle. The sides of the vehicle were divided into three bands, each one-third the height of the cylinder and divided into 6 zones of equal area. The angular divisions of the top, the bottom, and of each band coincide and fall at $a_s + 30^o$, $a_s + 90^o$, $a_s + 150^o$, $a_s + 210^o$, $a_s + 270^o$, and $a_s + 330^o$, where a_s is the azimuth angle of the sun. Thus, the symmetry of the choice of zones on the vessel allows the number of view-area calculations for each elevation angle to be reduced to 16 (excluding the simple G_s calculation for the zones on the top of the vessel). Another advantage of the symmetry is that it is necessary only to calculate view areas for sun elevation angles between 0^o and 90^o. The numbering of the zones is shown in Figure V-1.

B. CARD-TO-TAPE PROGRAM

The second program of the set is a card-to-tape program written in FORTRAN II for the IBM 1401. For inputs, this program requires sets of three output cards from the view-area program for the 16 zones mentioned above and for the 7 elevation angles: 0^o, 15^o, 30^o, 45^o, 60^o, 75^o, 90^o. The view-area program cannot perform calculations for the case of 0^o elevation of the sun. The view areas for 0^o elevation were calculated by extrapolation from the other view area calculations. Following this set of cards is one with a 4 in column 5, which indicates the end of the input data. The output from this program is a magnetic tape, written in 1401 internal notation, which contains a record for each set of three

input cards and a record for one zone on the top of the cylinder at each elevation angle. The information on each record is as follows:

$$n \text{ zone}, e\ell(\text{deg}), G_{em}, G_{es}, G_r, G_{rs}, G_s.$$

C. TEMPERATURE OF ZONES AND BOIL-OFF RATE

The final program of the set calculates the temperatures of the zones of the vessel and the percent boil-off of liquid hydrogen per year. Although we assumed that the lunar surface reflects solar radiation according to Hapke's photometric function, the calculations compare the temperatures calculated by using Hapke's formula with those calculated assuming a Lambert cosine reflector.

The temperatures of the zones are calculated by using Equation (V-54) and the heat flux into the storage vessel is computed by using Equation (V-56). The program also calculates the percentage of liquid hydrogen boil-off per year by using Equation (V-57).

The input data required for the program involving the heat flow equations (see section V-E) are given on four cards and the tape previously described. The first card has the data KON, AE, A,B,SF in the format:

I1, F9.4,3F10.4

where

KON = 0 (when Hapke view areas are used in the lunar surface reflectivity calculation) and

= 1 (when Lambert view areas are used),

AE = the absorptivity/emissivity ratio of the vessel shroud,

A = the albedo fraction for the lunar surface,

B = the particle reflectivity factor, and

SF = the shielding factor for the multilayer insulation.

The remaining cards give the conductance (in watts/°K) into the vessel for each zone in the format:

I1,F7.4,9F8.4

The integer in column 1 of these cards defines the zones on that card.

Column 1

2 conductance for zones 1 - 10 in order,

3 conductance for zones 11 - 20 in order,

4 conductance for zones 21 - 30 in order.

VII. PROGRAM RESULTS AND CONCLUSIONS

The numerical results of the analysis of the boil-off losses from a cryogenic vessel stored on the lunar surface are discussed in this section. The computer tabulations are shown in graphical form and the significant results are summarized.

Figures VII-1 and VII-4 show the view factors from the various zones of the vessel to the shaded and illuminated portions of the lunar surface. The view factor for solar radiation reflected from the lunar surface calculated from Lambert's law is greater than the view factor calculated from Hapke's photometric function. The lunar surface was assumed to be Lambertian in emission; therefore, the view factor for emitted infrared radiation from the lunar surface was calculated from Lambert's law.

Figures VII-5 shows the reflected solar radiation incident upon Zones 1, 2, 7, and 8 for various sun elevation angles according to computations using the Hapke photometric function. Zones 1 and 2 are located at the bottom and Zones 7 and 8 on the side of the vessel.

Figure VII-6 shows the radiative heat flux incident upon the outer shroud at various times during a lunation. The component of solar radiation reflected by the lunar surface according to the Hapke photometric function is small compared to the incident solar flux and the lunar surface thermal-emission components. However, for the assumed conditions the solar radiation reflected by the lunar surface according to Hapke's photometric function is about half that if the lunar surface were to reflect according to Lambert's law. We believe that this difference is caused by the strong retroreflection of a Hapke-type reflector.

The maximum incident solar flux is received by the outer shroud shortly after sunrise and shortly before sunset when both the top and the sides of the vessel are illuminated. The bottom of the vessel does not receive solar flux except during a period of about six minutes at sunrise and at sunset. A sharp decrease in the incident solar flux occurs at noon when the sides do not receive any solar radiation. This momentary shadowing has only a small effect on the outer shroud temperature. The calculations did not take into account the fact that the solar radiation is not collimated but subtends an angle of 32 minutes. For typical conditions, the error in the temperature of the outer shroud due to the assumption that the sunlight is collimated, is about .03°K.

The lunar surface thermal emission is the most significant component contributing to the heat flux incident upon the outer shroud. Because the exact magnitude of the lunar surface infrared emittance has not been established, an assumed emittance of unity will give conservative results. The magnitude of the total radiant heat flux incident upon the outer shroud of the cryogenic storage vessel is so large, compared to the flux due to sunlight reflected from the lunar surface, that the departure of the photometric function from Lambert's law is of slight importance.

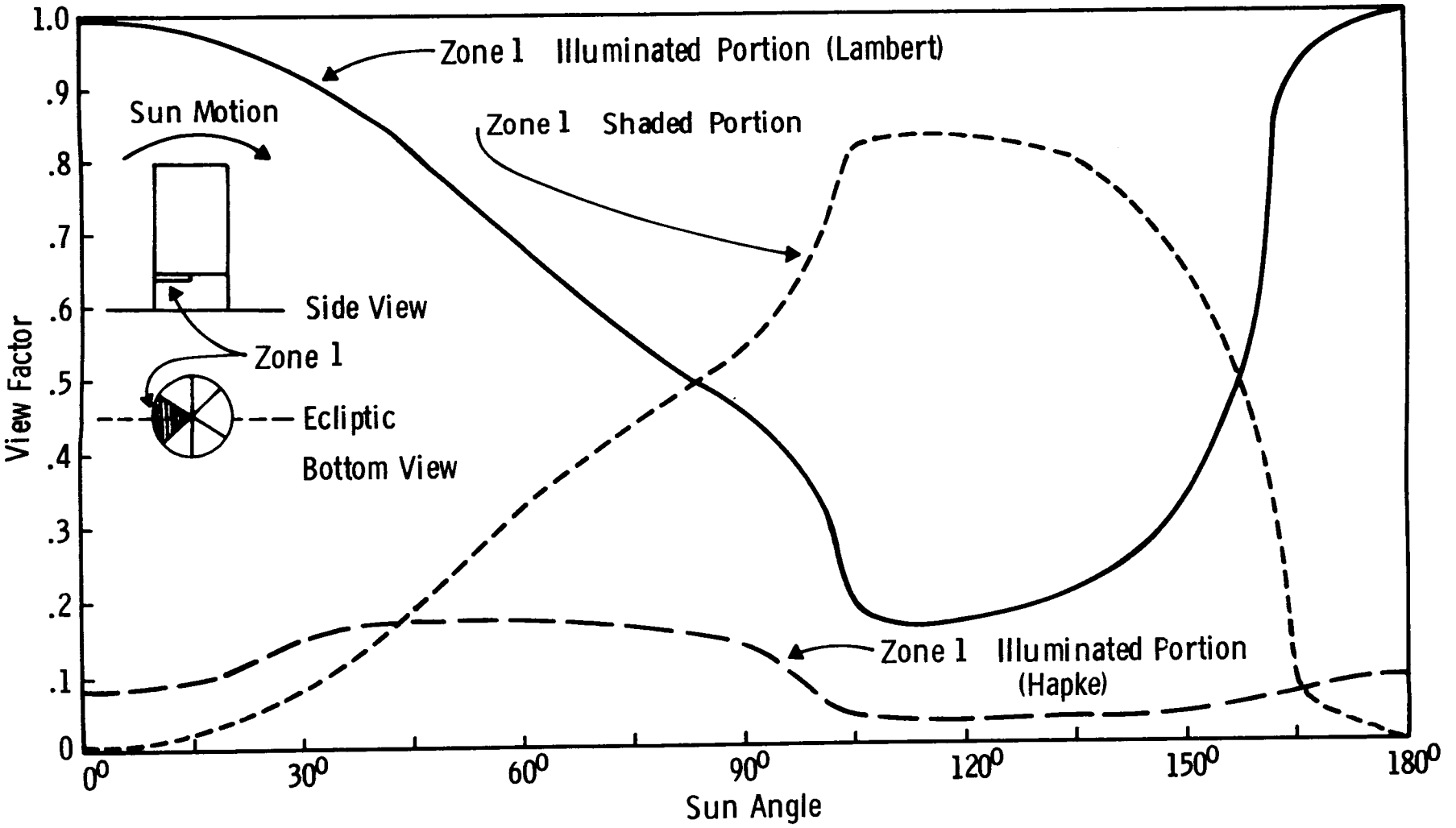

FIGURE VII-1 VIEW FACTOR OF ZONE 1 TO SHADED AND ILLUMINATED PORTIONS OF THE LUNAR SURFACE

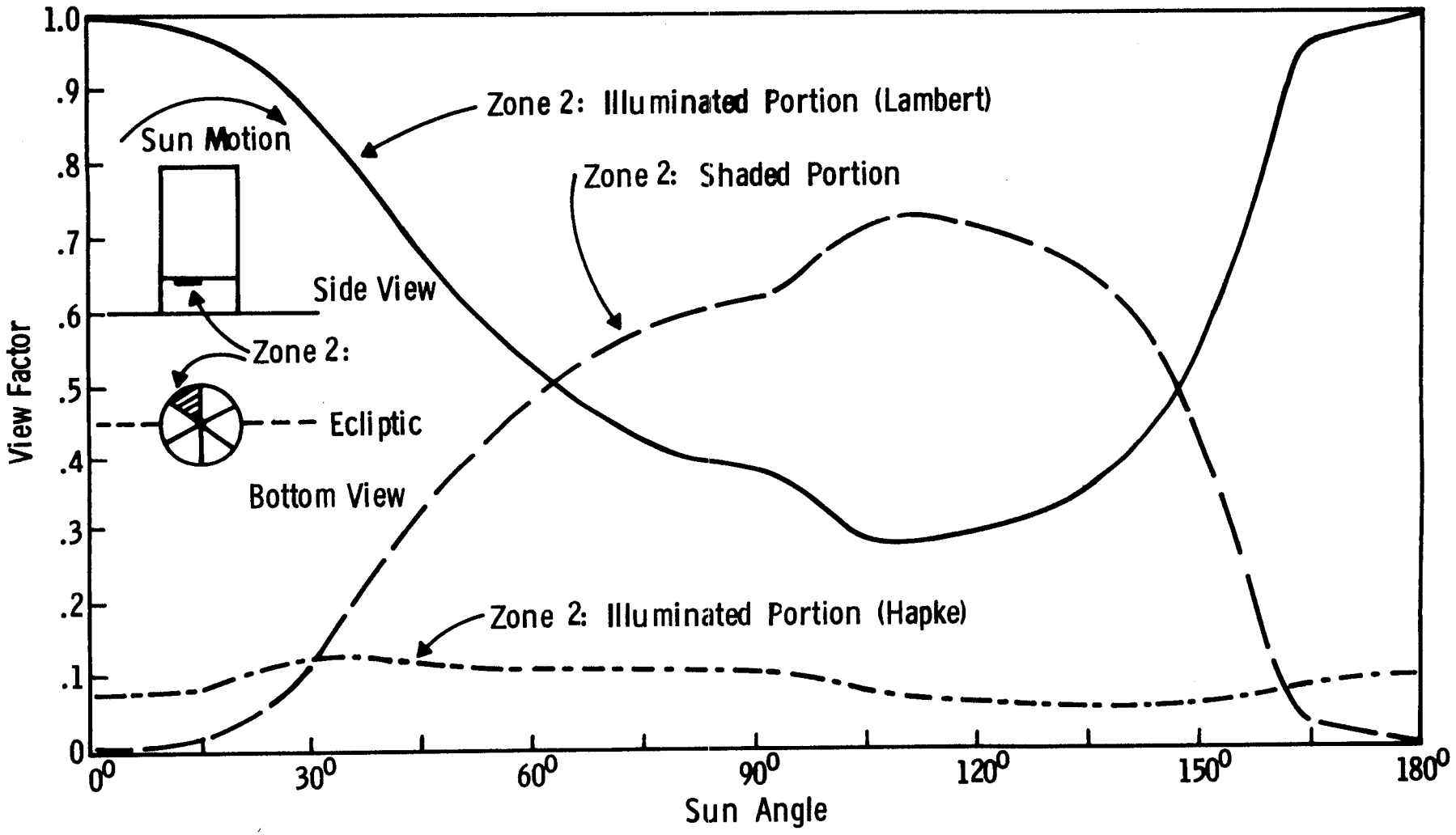

FIGURE VII-2 VIEW FACTORS OF ZONE 2 TO SHADED AND ILLUMINATED PORTIONS OF THE LUNAR SURFACE

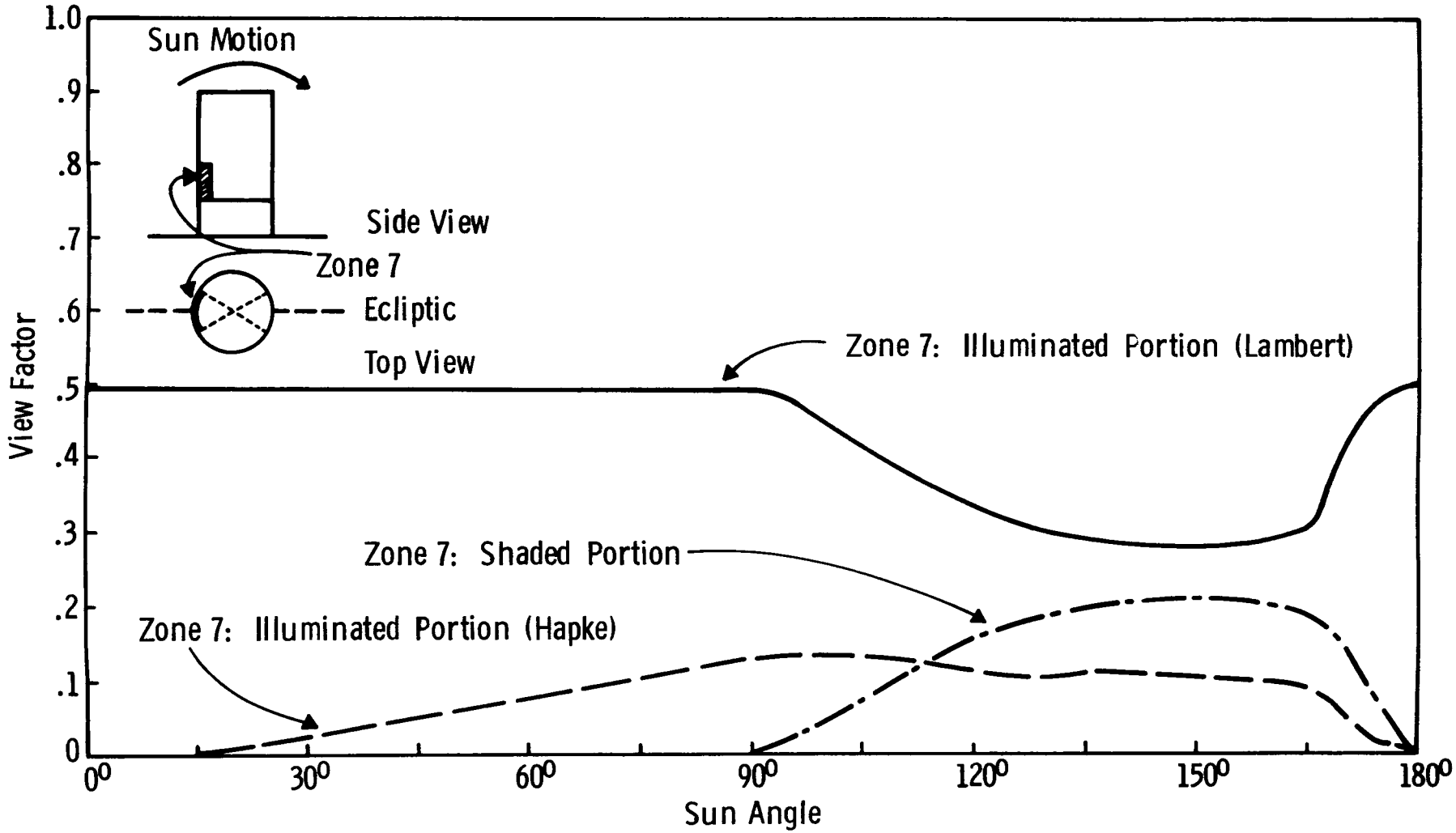

FIGURE VII-3 VIEW FACTORS OF ZONE 7 TO SHADED AND ILLUMINATED PORTIONS OF THE LUNAR SURFACE

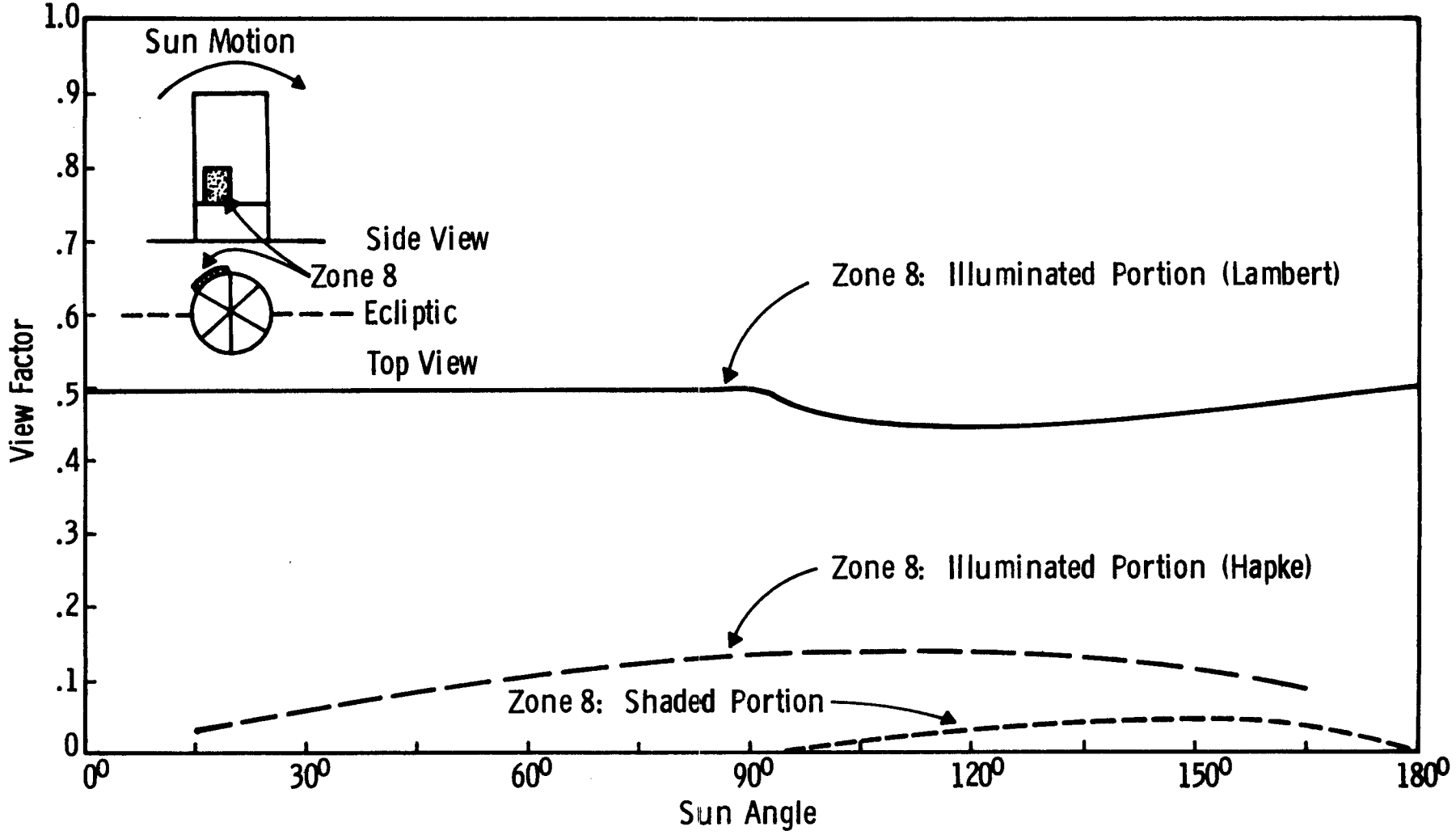

FIGURE VII-4 VIEW FACTORS OF ZONE 8 TO SHADED AND ILLUMINATED PORTIONS OF THE LUNAR SURFACE

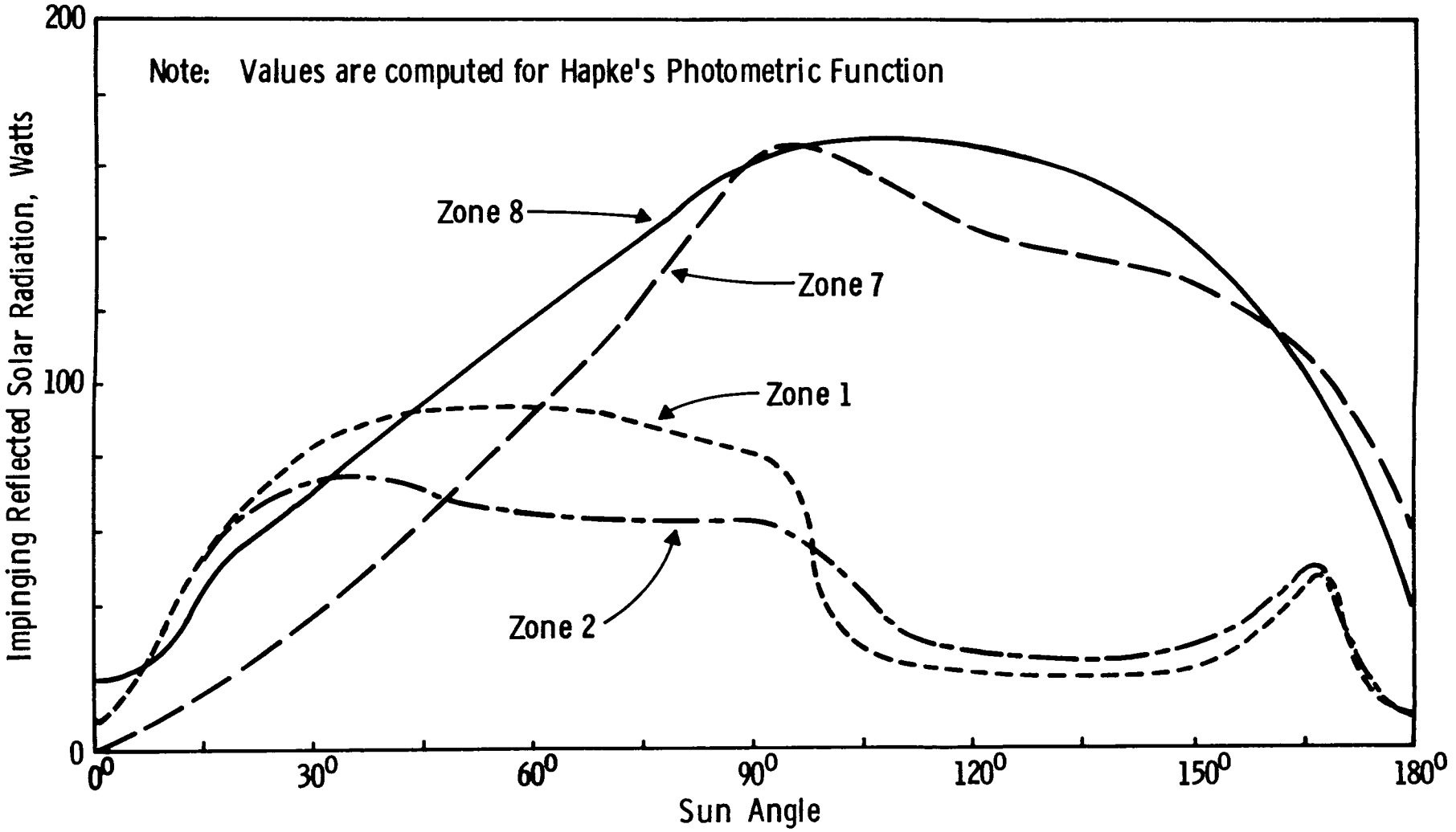

FIGURE VII-5 REFLECTED SOLAR RADIATION INCIDENT UPON ZONES 1, 2, 7 AND 8 VS SUN ELEVATION ANGLE

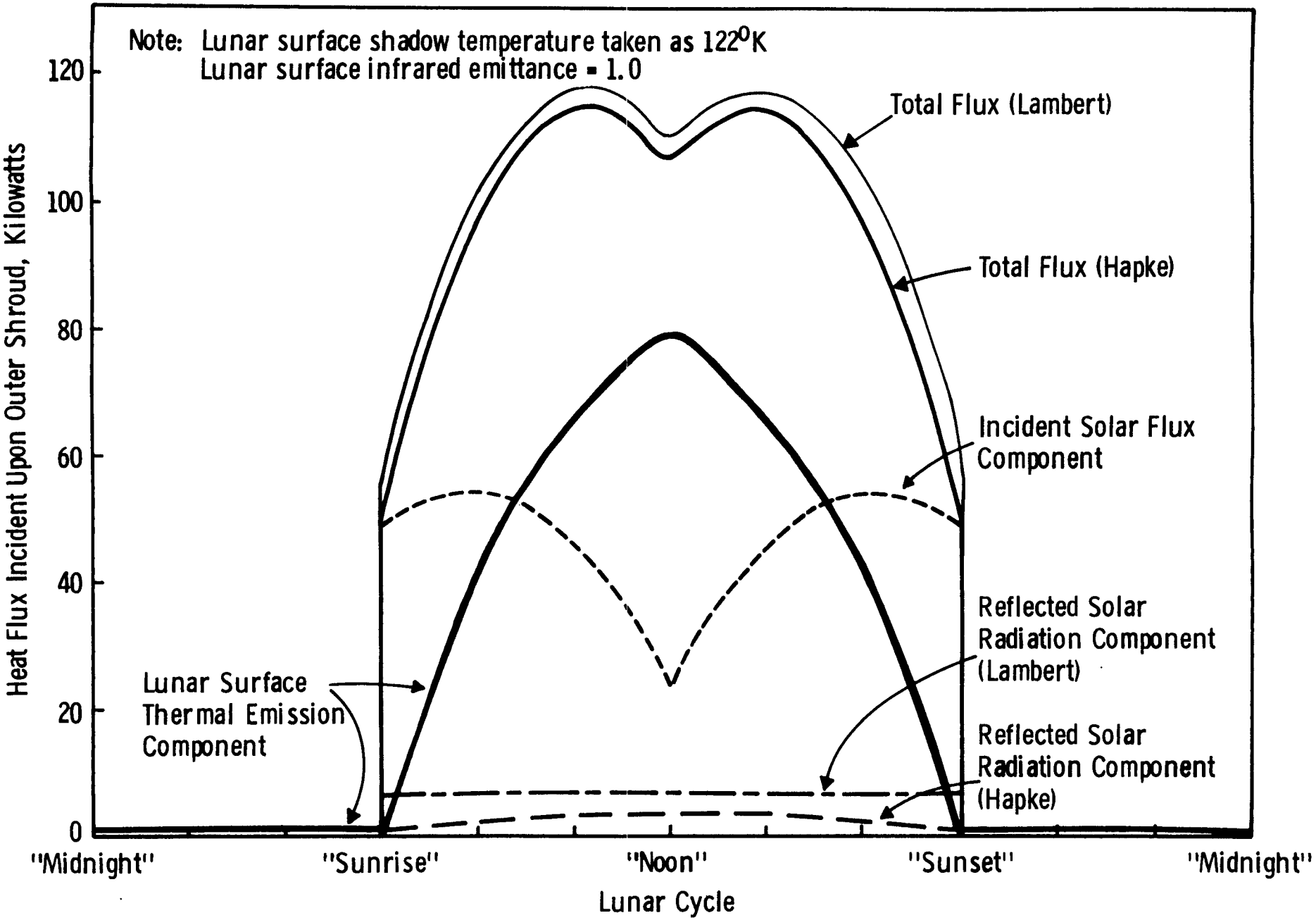

FIGURE VII-6 HEAT FLUX INCIDENT UPON OUTER SHROUD DURING A LUNATION

Table VII-I illustrates the effects of different lunar surface shadow temperatures on the total incident heat flux for Hapke's photometric function at different sun elevation angles. As these results indicate, the effects of the lunar surface shadow temperatures are negligible because of the small magnitude of the lunar surface thermal emission from the shadow.

Figures VII-7 and VII-8 show the boil-off rate in percent per year for different insulation shielding factors and various ratios of solar absorptance to infrared emittance of the outer shroud. These calculations are based on the assumption that the lunar surface reflects radiation according to Hapke's photometric function. For an insulation shielding factor of about 5,000, the boil-off rate would be in the order of 30% per year for a high α_s/ε ratio. Reductions in the boil-off rate for an insulation shielding factor greater than 15,000 are not very significant. Increased insulation shielding factors will result in an increase in weight and thickness of the insulation and thus detract from the advantages of a decrease in the boil-off rate. Even under the most optimistic conditions of very high insulation shielding factors and very low α_s/ε ratios, the boil-off rate would be about 7% per year for the model cryogenic vessel considered.

Figure VII-9 shows the dependence of the boil-off rate on the ratios of the outer shroud solar absorptance to infrared emittance for various penetration conductances and lunar surface reflection laws for an insulation shielding factor of 10,000. Instead of using a conductance, we used a shielding factor to characterize the heat flow through the insulation. This permits calculation of the heat flow through the insulation using the difference in T^4 instead of the difference in T. To be able to relate shielding factors to multilayer insulation systems, Figure VII-10 shows the dependence of shielding factors on different numbers of radiation shields and emittances, and Table VII-II gives typical thicknesses of multilayer insulations for different numbers of radiation shields.

The total penetration conductances, even though a small percentage of the effective insulation conductance, have an important effect on the boil-off rate. To illustrate the magnitude of the penetration and effective insulation conductance, let the insulation be exposed to a temperature of 300°K on its outer boundary and to 20.4°K on its inner boundary. For insulation shielding factors of 5,000, 10,000, and 20,000, effective conductances of the insulation are 47.2×10^{-3} watts/°K, 23.6×10^{-3} watts/°K, and 11.8×10^{-3} watts/°K respectively. The nominal conductance of the total penetration is 3.18×10^{-3} watts/°K.

TABLE VII-I

EFFECTS OF LUNAR SURFACE SHADOW TEMPERATURES
ON TOTAL INCIDENT HEAT FLUX (HAPKE)

Sun Elevation Angle	(Kilowatts) T_{min} = 122°K	T_{min} = 100°K	T_{min} = 80°K
0°	49.68	49.19	48.95
15°	77.65	77.62	77.60
30°	97.11	97.05	97.02
45°	109.15	109.07	109.03
60°	114.67	114.59	114.55
75°	113.61	113.52	113.48
90°	106.90	106.83	106.80

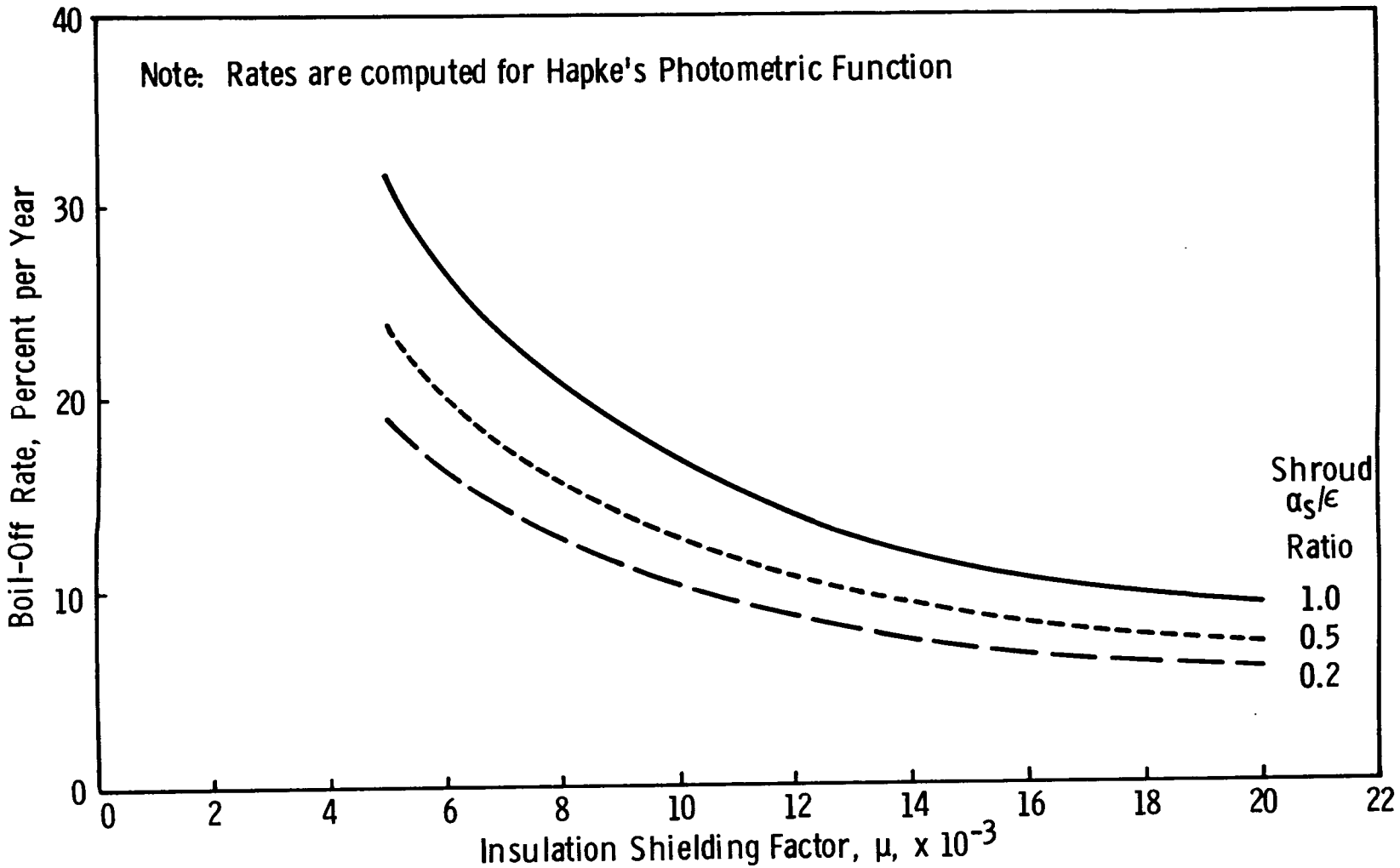

FIGURE VII-7 BOIL-OFF RATE VS INSULATION SHIELDING FACTOR FOR VARIOUS OUTER SHROUD SOLAR ABSORPTANCE TO INFRARED EMITTANCE RATIOS

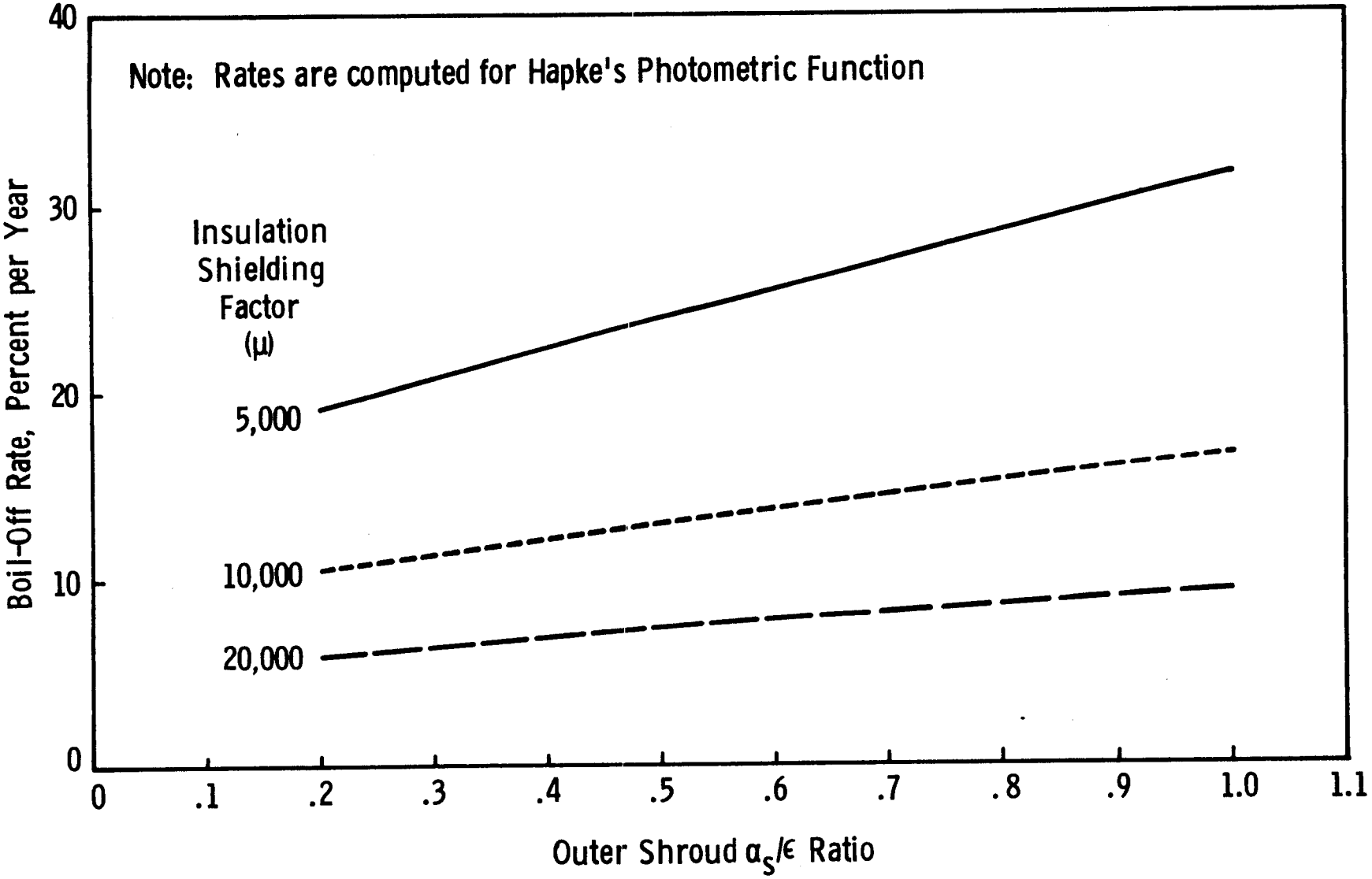

FIGURE VII-8 BOIL-OFF RATE VS OUTER SHROUD SOLAR ABSORPTANCE TO INFRARED EMITTANCE RATIO FOR VARIOUS INSULATION SHIELDING FACTORS

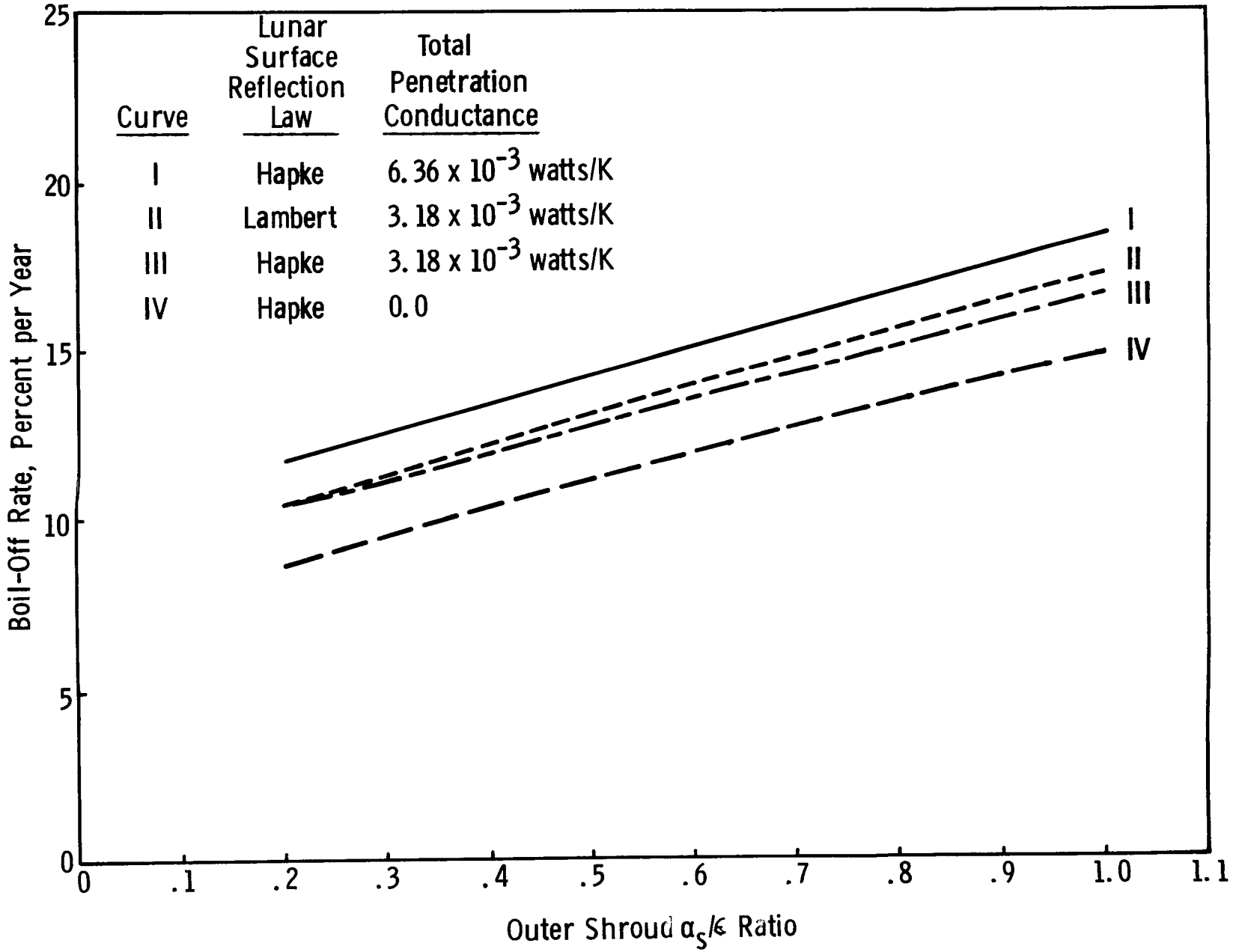

FIGURE VII-9 BOIL-OFF RATE VS OUTER SHROUD SOLAR ABSORPTANCE TO INFRARED EMITTANCE RATIO FOR VARIOUS PENETRATIONS AND LUNAR SURFACE REFLECTION LAWS

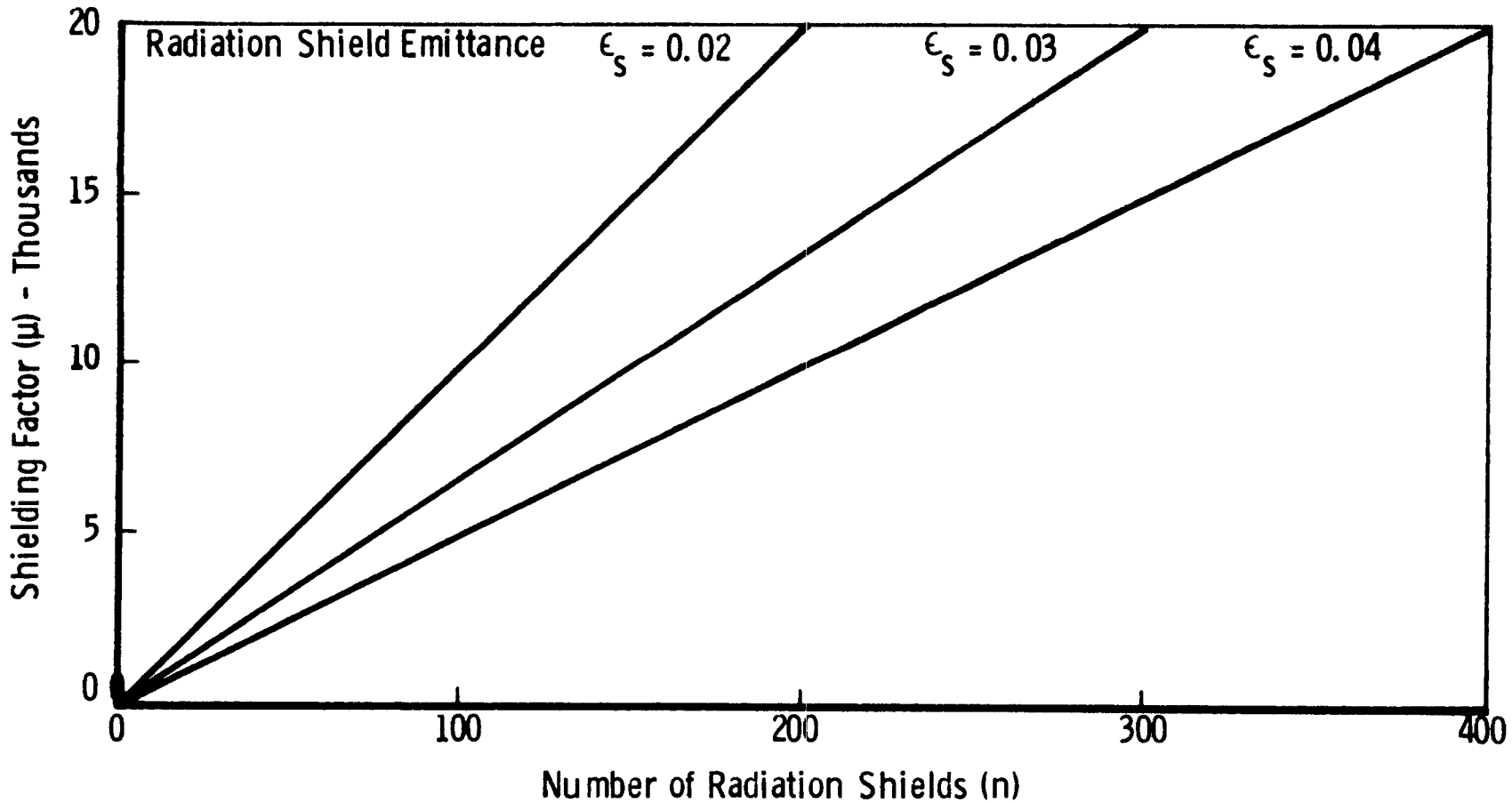

FIGURE VII-10 DEPENDENCE OF SHIELDING FACTORS ON DIFFERENT NUMBERS OF RADIATION SHIELDS AND EMITTANCES

TABLE VII-II

TYPICAL THICKNESSES OF MULTILAYER INSULATIONS
FOR DIFFERENT NUMBERS OF RADIATION SHIELDS

Number of Radiation Shields	Multilayer Insulation Thickness		
	.007" Thick Netting Nylon	Crinkled Polyester Film	.003" Thick Glass Fiber Paper
50	0.95"	0.75"	1.35"
100	1.90"	1.50"	2.70"
200	3.80"	3.00"	5.40"
300	5.70"	4.50"	8.10"
400	7.60"	6.00"	10.80"

APPENDIX A

EFFECTS OF SKIN CONDUCTANCE AND THERMAL MASS

A one-dimensional, transient thermal analysis of the heat flow in the skin was made to test the assumption that the conductance of the outer skin of the vessel and the thermal mass of the skin do not appreciably influence the heat flux into the vessel. We define the thermal mass of an object to be the product of the heat capacity and the inertial mass of the object.

The temperature distributions in a section of the skin were calculated by using the "Method of Zones" (Strong and Emslie, 1965) for two situations:

(a) Case I -- The skin was assumed to have a finite azimuthal conductance and thermal mass.

(b) Case II -- The skin was assumed to be non-conducting and to have no thermal mass.

The temperature distributions were calculated without considering a thermal conductance between the skin and cryogen.

Figure A-1 shows the dimensions of the skin section, assumed to be made of 6061 aluminum and to have the following characteristics:

Thickness	- 0.159 cm (1/16")
Conductivity	- 1.5 watts/cm-K
Density	- 2.7 g/cc
Specific Heat	- 1.0 joule/g-K

The section of skin was taken to be 244 centimeters in height and was subdivided azimuthally into 6 zones. As shown in Figure A-1, because of the symmetry of the problem, only six zones are required to compute the temperature distribution. Heat-balance equations were written in order to compute the temperature history of each zone and the seven boundary temperatures. The equations were solved by use of the Arthur D. Little, Inc. Transient Thermal Analysis Computer Program.

A special program was written to compute the heat flux from the skin to the insulated cryogenic vessel. The heat flux into the vessel was computed from the mean temperatures of the six zones by using the following equation:

$$q = \sum_{i=i}^{n} \frac{Ai}{\mu} \sigma \int (T_i^4(t) - T_{H_2}^4)\, dt \qquad (1)$$

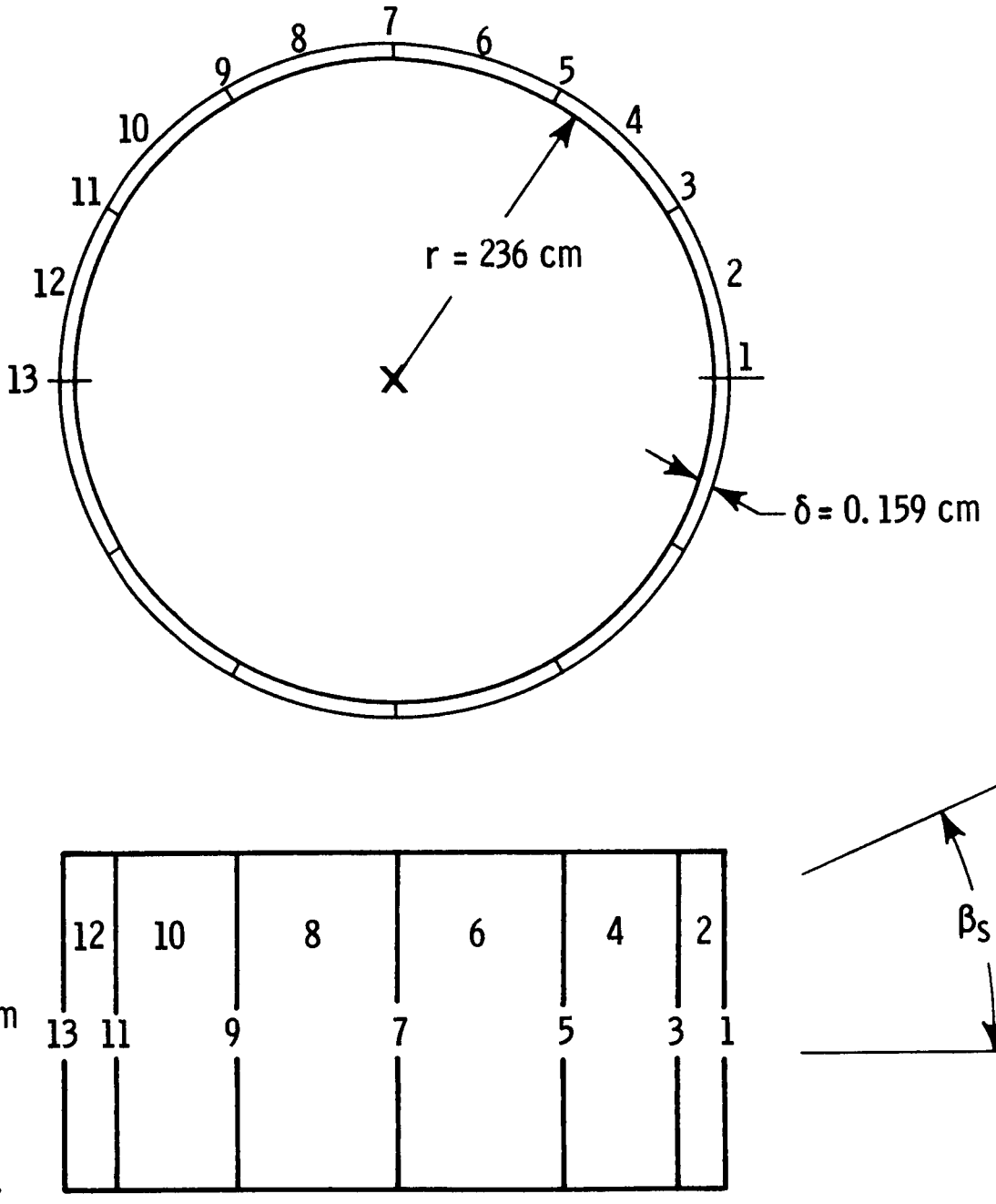

Note: Numbers on diagram identify temperatures used in the calculations.

FIGURE A-1 DIAGRAM OF SKIN SECTION

where q - total heat flux (watts)

A_i - area of zone (cm^2)

μ - shielding factor

n - number of zones

T_i - mean temperature of skin (K)

T_{H_2} - assumed temperature of LH_2 (20.4 K)

t - time

The computations of the total heat flux for the two cases were made for a time period of 13.65 days and, to accentuate the differences between the two cases, direct sunlight was the only input power considered for this example. The solar absorptance-to-emittance ratio of the external surface of the skin was taken to be 1.0; the shielding factor, 10,000. The time interval used in the calculations of the transient temperatures of the skin was 6.8 minutes.

Figure A-2 shows a graph of the temperatures calculated for zone 2. The inclusion of thermal mass and azimuthal conductance has negligible effect except during the time when the zone is shadowed from direct sunlight. If the other two sources of incident power (reflected sunlight and infrared radiation emitted from the lunar surface) had been included, the differences in calculated temperatures between Cases I and II would be negligible.

Although the temperatures of the skin are different for the two cases when the zone is shadowed, the heat flux into the cryogenic storage vessel is nearly the same for both cases because the total heat flux is almost entirely carried by the flux leaking in from the illuminated side of the vessel. For the particular situation described, the ratio of the total heat leaks for the two cases was calculated to be

$$\frac{q_I}{q_{II}} = 0.97$$

where q_I is the calculated heat leak to the storage vessel for a finite skin conductance and thermal mass, and q_{II} is the calculated heat leak when the thermal mass and azimuthal conductance of the skin are neglected. For all practical purposes, the 3% error will not be important since the uncertainty in shielding factor alone will result in larger uncertainties in the computed heat leak.

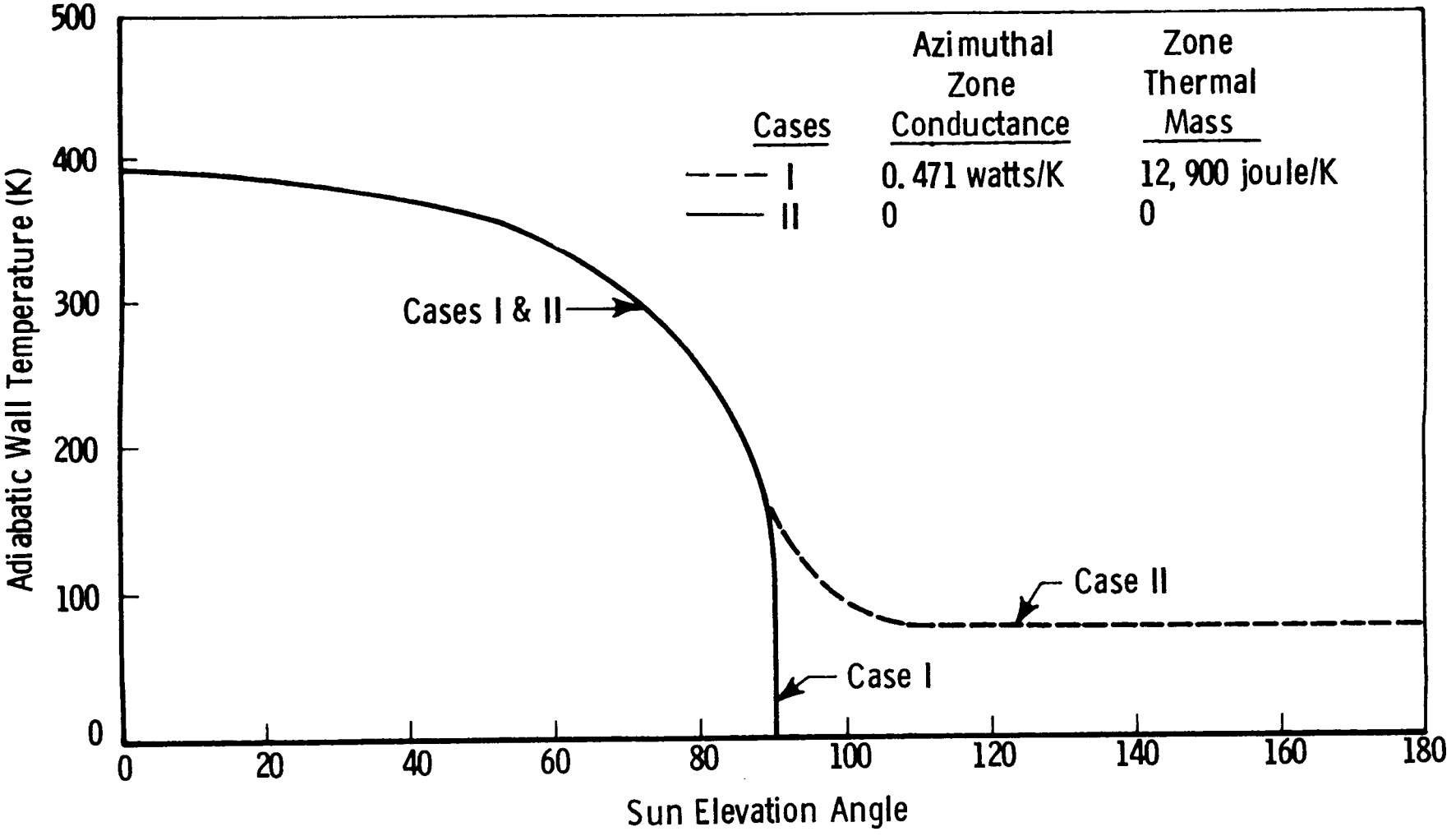

FIGURE A-2 TYPICAL SKIN TEMPERATURE HISTORY, ZONE 2

We also wish to investigate the validity of the assumption that the thermal mass of the insulation does not significantly affect the average heat leak into the cryogenic storage vessel. The behavior of the insulation during the initial transient will not be considered, since this depends on the temperature distributions existing during the transfer orbit. We will, therefore, analyze the periodic behavior of the insulation, since the storage vessel is expected to remain on the lunar surface for about one year.

We will characterize the insulation by an effective thermal conductivity K, an effective density , heat capacity c and thickness a. While the conductivity of typical insulations is a function of temperature, we will use a linear model in order to make the analysis possible.

The temperature, T, of the insulation is determined by the usual diffusion equation

$$C\rho \frac{\partial T}{\partial t} = K \frac{\partial^2 T}{\partial x^2} \qquad (2)$$

where t is the time
x is the coordinate normal to the insulation, with origin at the outside skin.

The general periodic solution to Equation 2 is

$$T = \sum_{n=1}^{\infty} (T_n e^{i\gamma_n x} + T_{-n} e^{i\gamma_n x}) e^{inwt} + T_o - Ax \qquad (3)$$

where

T_n, T_{-n} are Fourier series coefficients determined from the boundary conditions

$$\gamma_n = \sqrt{\frac{nwC\rho}{iK}}$$

T_o is the average temperature of the skin

$$A = \frac{T_o - T_{H_2}}{a}$$

T_{H_2} is the temperature of the cryogen, a constant.

The heat flux, q, at the inner wall of the vessel, x = a, is given by the expression

$$q = -K \left[\frac{\partial T}{\partial x}\right]_a = -K \left\{ \sum_{n=1}^{\infty} i\gamma_n \left(T_n e^{i\gamma_n a} - T_{-n} e^{-i\gamma_n a}\right) e^{inwt} - A \right\} \quad (4)$$

Clearly the terms with the periodically varying factors e^{inwt} will drop out when the value of $\bar{q}$ is obtained by averaging q over a period. Therefore,

$$\bar{q} = KA \quad (5)$$

and thus the average flux to the cryogen is independent of the heat capacity of the shielding.

APPENDIX B

SHIELDING FACTOR

In a discussion of evacuated multilayer insulation systems applied to cryogenic storage vessels it is convenient to define a single parameter which can be used to characterize the thermal performance of the insulation system.

For example, consider the case of a system of "floating" radiation shields interposed between an outer skin whose temperature is T_s and a cryogenic storage vessel whose temperature is T_t, as shown in the following sketch.

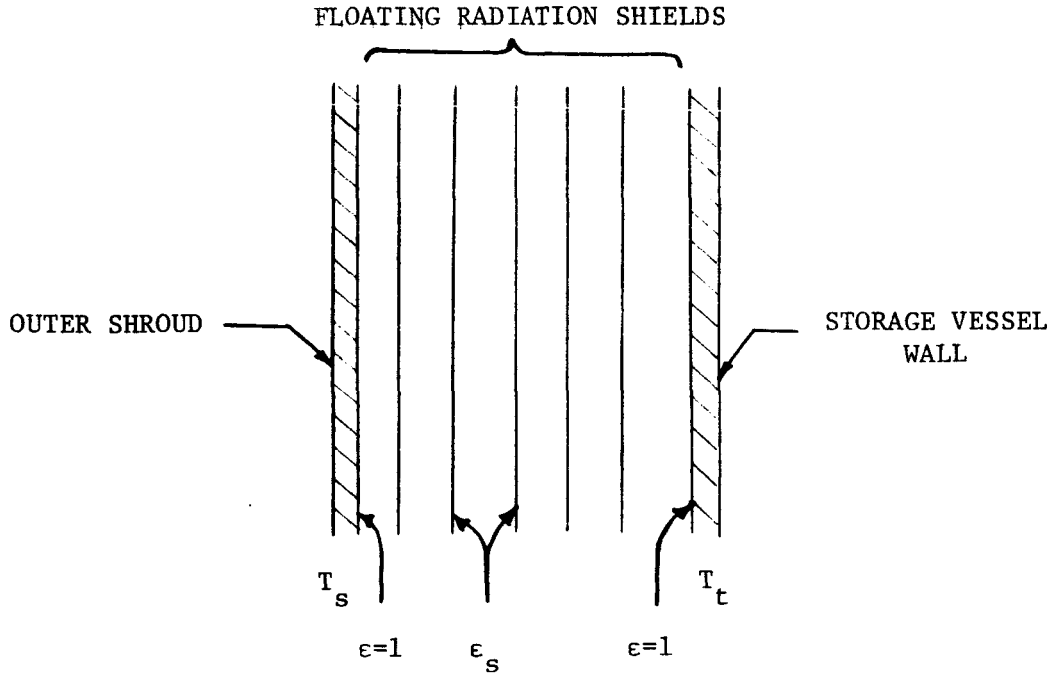

We assume that the emittance of each shield is ε_s and that the outer shroud and storage vessel surfaces have an emittance of unity. The net rate of heat flow between the outer shroud and the storage vessel wall for a system of floating radiation shields is given by the expression

$$\frac{q}{A} = \frac{\sigma T_s^4 - \sigma T_e^4}{2n/\varepsilon_s + 1}$$

where $\frac{q}{A}$ = heat flux (in watts/cm^2)

n = number of floating radiation shields

ε_s = shield emittance

T_s = outer shroud temperature

T_t = storage vessel wall temperature

We define a shielding factor μ as

$$\mu = 2n/\varepsilon_s + 1$$

For a typical cryogenic insulation system which utilizes a multiplicity of low emittance shields the above equation can be approximated by the expression

$$\mu \simeq \frac{2n}{\varepsilon_s}$$

For a typical case of 200 shields of emittance $\varepsilon_s = 0.04$, the shielding factor is

$$\mu = 10{,}000$$

In any real system of shields, there is, of course, conduction of heat between the shields. For multilayer insulation systems, the value of the shielding factor is experimentally determined by calorimetric methods (Black et al, 1964). It is found that the shielding factor is very near the value calculated when conduction is ignored.

APPENDIX C

WALL TEMPERATURE

We define an adiabatic wall temperature as one where all conductive heat fluxes are neglected. For purposes of calculating the heat flux to a highly insulated cryogenic storage tank this method has been treated by Bonneville (1964).

Consider a unit area of the surface of a highly insulated cryogenic storage tank to be illuminated by a constant radiative flux, S, and let the absorptance and emittance of the outer skin be α_o and ε, respectively.

The skin is assumed to be separated from the cryogenic storage vessel by a multilayer insulation whose effectiveness is characterized by a shielding factor .

From the heat balance on the outer skin we find the expression

$$\varepsilon \sigma T_s^4 + \frac{1}{\mu} (\sigma T_s^4 - \sigma T_o^4) = \alpha_o S$$

where

T_s - outer skin temperature

μ - insulation shielding factor

T_o - cryogen temperature

S - incident heat flux

We define the adiabatic wall temperature, T_{sa}, such that it satisfies the equation

$$\sigma T_{sa}^4 = \frac{\alpha_o}{\varepsilon} S$$

The term $\frac{1}{\mu} (\sigma T_s^4 - \sigma T_o^4)$ in the heat balance equation represents the net rate of heat flow to the cryogen, and if this term is small with respect to the flux emitted to outer space $\varepsilon\sigma T_s^4$, we find that

$$T_s \simeq T_{sa}$$

We also note that the adiabatic wall temperature is independent of the magnitudes of the emittance and absorptance.

The error involved in calculating the temperature when the heat flux to the cryogen is neglected can be easily calculated for a typical cryogenic storage vessel where the shielding factor μ is a large number and

$$T_s^4 >> T_o^4$$

Combining equations, we find that

$$\frac{T_{sa}^4}{T_s^4} \simeq 1 + \frac{1}{\mu\epsilon}$$

Taking a typical value of $\mu = 10{,}000$ and $\epsilon = 1.0$, we find that the error in the fourth power of the temperature is 0.01%. This is also the error introduced in the computation of the heat flux to the stored cryogen if the adiabatic temperature instead of the actual skin temperature is used to calculate the inward heat flux.

The error in the temperature may be calculated by expanding about the temperature T_s.

Let $T_{sa} = T_s + \Delta T$

Then $\sigma T_{sa}^4 \simeq \sigma T_s^4 + 4 \sigma T_s^3 \Delta T$

and $\Delta T \simeq \frac{1}{\mu\epsilon} \frac{T_s}{4}$

For $\epsilon = 1.0$

$\mu = 10{,}000$

$T_s = 397^\circ K$

we find that

$$T_{sa} - T_s = 0.01^\circ K$$

i.e., an error of 0.0025% in absolute temperature.

Because the shielding factors used in this example are typical of an insulated vessel on the surface of the moon, the adiabatic wall temperature can be used in place of the skin temperature in calculating the boil-off of the cryogen in the vessel.

REFERENCES

Aranowitz, L. and Milford, S.N.: Magnetic Shielding of the Lunar Surface from the Solar Wind as a Function of Lunar Magnetic Moment, J. Geophys. R., vol. 70, 1965, pp. 227-229.

Arvesen, J.C. and Hamaker, F.M.: Effectiveness of Radiation Shields for Thermal Control of Vehicles on the Sunlit Side of the Moon, NASA TN D-2130, April 1964.

Baldwin, R.P.: The Measure of the Moon, University of Chicago Pr., 1962.

Barabashov, N.P. and Garazha, V.I.: The Microstructure of the Lunar Surface, Soviet Astron., vol. 6, 2, Sept. - Oct. 1962.

Bjork, E.L.: Analysis of the Formation of Meteor Crater Arizona, A Preliminary Report, J. Geophys. Rev., vol 66, 1961, pp. 3379-3387.

Black, I.A. and Glaser, P.E.: The Performance of a Double-Guarded Cold-Plate Thermal Conductivity Apparatus, Advances in Cryogenic Eng., Vol. 9, pp. 52-63, 1964, Ed.-K. D. Timmerhaus - Plenum Pr., N. Y.

Buna, T.: Thermal Aspects of Long-Term Propellant Storage on the Moon, Jour. Spacecraft and Rockets, vol. 1, 1964, pp. 484-491.

Carslaw, H.S. and Jaeger, J.C.: Conduction of Heat in Solids, 2nd Ed., Clarendon Pr. (Oxford) 1959.

Coffman, M.L.: Charging Grains of Dust, J. Geophys. Res., vol. 8, 1963, pp. 1565-1566.

Costain, C.H., Ellsmore, B. and Whitfield, G.R.: Radio Observations of a Lunar Occultation of the Crab Nebula, N.M., vol. 116, 1955, pp. 380-385.

Dempster, W.E., Evans, R.L. and Olivier, J.R.: Lunar Storage of Liquid Propellants, NASA TN D-1117, July 1962.

Dollfus, A.: Nouvelle Recherche d'une Atmosphere au Voisinage de la Lune, C. R., vol.234, 1952, pp. 2046-2049.

Fessenkov, V.G.: Photometry of the Moon. Physics and Astronomy of the Moon, Z. Kopal, ed., Academic Pr., 1962, pp.

Gault, D.E., Shoemaker, E.N., and Moore, H.J.: Spray Ejected from the Lunar Surface by Meteoroid Impact, NASA TN D-1767, 1963.

Gehrels, T.: A Model of the Lunar Surface. Icarus, vol. 3, 1964, pp. 491-496.

Glaser, P.E., ed.: Studies of the Physical Characteristics of Probable Lunar Surface Materials, Part II. Final Report. Arthur D. Little, Inc. (AF 19(628)-421) (AFCRL-64-970 (II)), 1964.

Glaser, P.E., Wechsler, A.E., and Germeles, A.E.: Thermal Properties of Postulated Lunar Surface Materials. Ann. N.Y. Acad. Sci., vol.123, no. 2, 1965, pp. 656-670.

Grannis, P.D.: Electrostatic Erosion Mechanisms on the Moon. J. Geophys. Res., vol. 66, 1961, pp. 4293-4299.

Green, J.: Tital and Gravity Effects Intensifying Lunar Defluidization and Volcanism. Ann. N.Y. Acad. Sci., vol.123, no. 2, 1965, pp. 406-469 .

Hagfors, T, Brockelman, R.A., Danforth, H.D., Hanson, L. B., and Hyde, G.M.: Tenuous Surface Layer on the Moon: Evidence Derived from Radar Observations. Science, vol. 150, No. 3700, pp. 1153-56, 1965.

Halajian, J.D.: Photometric Measurements of Simulated Lunar Surfaces. NASA Contract No. NAS9-3182, July, 1965.

Hapke, B.: Effects of a Simulated Solar Wind on the Photometric Properties of Rocks and Powders. Ann. N.Y. Acad. Sci., Vol. 123, No. 2, 1965, pp. 711-721.

Hapke, B., and Van Horn, H.: Photometric Studies of Complex Surfaces, with Applications to the Moon. J. Geophys. Res., vol. 68, 1963, pp. 4545-4570.

Hapke, B.: A Theoretical Photometric Function for the Lunar Surface, Ibid, pp. 4571-4586, 1963.

Henry, R.L.: The Transmission of Powder Films in the Infra-red. J. Opt. Soc. Am., Vol. 38, 1948, p. 775.

Ingrao, H.C., Young, A. T., and Linsky, J.L.: A Critical Analysis of Lunar Temperature Measurements in the Infrared. Harvard College Observatory. NASA Res. Grant No. NsG-64-60, April 1965.

Jaeger, J.C.: The Surface Temperature of the Moon. Aust. J. Physics, vol. 6, pp. 10-17.

Krotikov, V.D. and Shchuko, O.B.: The Heat Balance of the Lunar Surface During a Lunation. Soviet Astron.-A.J., vol. 7, 1963, p. 228.

Kubelka, P.: New Contributions to the Optics of Intensely Light-Scattering Materials, Pt. I. J. Opt. Soc. Am., vol. 38, 1948, p. 448.

Leonhard, K.E.: Seminar Discussion, Eleventh Cryogenic Conf., Houston, 1965.

Little, (Arthur D.) Inc.: Basic Investigations of Multilayer Insulation Systems. Final Report. Cont. No. NAS3-4181, NASA CR-54191, 1964.

Little, (Arthur D.) Inc.: Liquid Propellant Losses During Space Flight. Final Report. Cont. No. NASw-615. Report No. 65008-00-04, 1963.

Lockheed Missiles and Space Co., Sunnyvale, Calif.: Development of Thermal Protection Systems for a Cryogenic Spacecraft Module (NAS3-4199), 1965.

Low, F.J.: Planetary Atmospheres at One Millimeter and Shorter Wave Lengths. Symposium on Millimeter Wave Techniques in Space Electronics, Cambridge, Massachusetts, May 1965.

Lyon, R.J.P.: Evaluation of Infrared Spectrophotometry for Compositional Analysis of Lunar and Planetary Soils. Stanford Res. Inst. NASA Cont. No. NASr-49(04), 1962.

Markov, M.N. and Khokhlova, V.L.: Coefficients of Emission in the Infrared Region of the Spectrum and Differences in the Parameter $\lambda = (k_\rho c)^{-\frac{1}{2}}$ for the Sea and Continent Regions of the Lunar Surface. Sov. Phys.-Doklady, vol. 9, Feb. 1965, pp. 621-624.

McCracken, C.W. and Dubin, M.: Dust Bombardment on the Lunar Surface. The Lunar Surface Layer. J.W. Salisbury and P.E. Glaser, eds., Academic Pr., 1964, pp. 179-214.

Meissner, H.P., Michaels, A.S., and Kaiser, R.: Spontaneous Pelletization in Fine Powders. Indus. Eng. Chem. Proc. Design and Dev., vol. 3, 1964, pp. 197-202.

Merrill, R.B.: The Effects of Micrometeoroids on the Emittance of Solids. Thermal Radiation of Solids, NASA SP-55, 1965, pp. 453-472.

Mirtich, M.J. and Mark, H.: Alteration of Surface Optical Properties by High Speed Micron-Size Particles, ibid, pp. 473-481.

NASA: Solar Proton Manual, TRR-169, Sept. 1963.

Opik, E.J. and Singer, S.F.: Escape of Gases from the Moon. J. Geophys. Res., vol. 65, 1960, pp. 3065-3070.

Opik, E.J.: The Lunar Atmosphere. Planetary and Space Sci., vol. 9, 1962, pp. 211-244.

Paivanos, J.A., Roberts, O.P., and Wang. D.I.J.: Multi-Shielding - An Advanced Super Insulation Technique. Advances in Cryogenic Engineering, vol. 10, Plenum Pr. 1965, pp. 197-207.

Perkins, P.J., Coluca, M.A., and Smith, L.S.: Preliminary Test Results in a Compressed Multi-Layer Insulation System for a Liquid-Hydrogen-Fueled Rocket. Advances in Cryogenic Engineering, vol. 9, Plenum Pr. 1964, pp. 38-45.

Pettit, E. and Nicholson, S.B.: Lunar Radiation and Temperature, Astrophys. J., vol. 71, 1930, p. 102.

Polgare, G.L. and Howell, J.R.: The Directional Radiative Characteristics of Conical Cavities and Their Relation to Lunar Phenomena. AIAA Paper No. 65-669, AIAA Thermophysics Specialist Conf., Monterey, Calif., Sept. 1965.

Pythagore Technique, The: Gazocean-Technigaz, Paris, 1965.

Romero, J.B., Smith, D.W., and Dod, R.E.: Thermal Analysis and Optimization of Cryogenic Tanks for Lunar Storage. Presented at Cryogenic Eng. Conf., Houston, Texas, August, 1965, Paper E-6.

Salisbury, J.W., Glaser, P.E., Stein, B.A., and Vonnegut, B.: Adhesive Behavior of Silicate Powders in Ultra-high Vacuum. J. Geophys. Res., Vol. 69, 1964, pp. 235-242.

Salisbury, J.W. and Smalley, V.G.: The Lunar Surface Layer. J.W. Salisbury and P.E. Glaser, Eds., Academic Pr., 1964, pp. 411-443.

Salisbury, J.W. and Glaser, P.E., Eds.: Studies of the Characteristics of Probable Lunar Surface Materials. AFCRL and Arthur D. Little, Inc. AF 19(628)-421. AFCRL-64-970, 1963, p.3.

Scott, R. B.: Cryogenic Engineering. Van Nostrand, 1959, p. 235.

Shorthill, R.W. and Saari, J.M.: Radiometric and Photometric Mapping of the Moon through a Lunation. Ann. N.Y. Acad. Sci., vol. 123, no. 2, 1965, pp. 722-739.

Singer, S.F. and Walker, E.H.: Electrostatic Dust Transport on the Lunar Surface. Icarus, vol. 1, 1962, pp. 112-120.

Smoluchowski, R.: Radiation Sintering of Lunar Dust. Science, vol. 150, 1965, pp. 1025-1026.

Strong, P. F. and Emslie, A.G.: The Method of Zones for the Calculation of Temperature Distribution. Presented at ASME Mtg., Chicago, Ill., November 1965, Paper No. 65-WA/HT-47.

Sytinskaya, N.N.: New Data on the Meteoric Slag Theory of the Formation of the Outer Layer of the Lunar Surface. Soviet Astron.-A.J., vol. 3, 1959, p. 310.

Timmerhaus, K.D., ed.: Advances in Cryogenic Engineering, Plenum Pr., 1958-1965.

Urey, H.C.: On Possible Parent Substances for the C_2 Molecules Observed in the Alphonsus Crater. Astrophys. J., vol. 134, 1961, pp. 268-269.

Van Tassel, R.A. and Simon, I.: Thermal Emission Characteristics of Mineral Dusts. The Lunar Surface, J.W. Salisbury and P.E. Glaser, Eds., Academic Pr., 1964, pp. 445-468.

Walker, E.H.: Comments on a Paper by P.D. Grannis. J. Geophys. Res. vol. 67, 1962, pp. 2586-2587.

Watson, J., Murray, B.C., and Grown, H.: The Behavior of Volatiles on the Lunar Surface. J. Geophys. Res., vol. 60, 1961, pp. 3033-3047.

Whipple, F.L.: The Dust and Cloud about the Earth. Nature, vol. 189, 1961, pp. 127-128.

Whipple, F.L.: On Meteoroids and Penetration. J. Geophys. Res., vol. 68, 1963, pp. 4929, 4940.